Journal of Molecular Liquids 218 (2016) 16–34

Contents lists available at ScienceDirect

Journal of Molecular Liquids

journal homepage: www.elsevier.com/locate/molliq

Geometrical structures, thermal properties and antimicrobial activity studies of azodye complexes

A.Z. El-Sonbati [a,*], A.A. El-Bindary [a], G.G. Mohamed [b], Sh.M. Morgan [c], W.M.I. Hassan [b], A.K. Elkholy [a]

[a] Chemistry Department, Faculty of Science, Damietta University, Damietta, Egypt
[b] Chemistry Department, Faculty of Science, Cairo University, Giza, Egypt
[c] Environmental Monitoring Laboratory, Ministry of Health, Port Said, Egypt

ARTICLE INFO

Article history:
Received 10 December 2015
Accepted 9 February 2016
Available online xxxx

Keywords:
Metal complexes
Molecular structures
Quantum chemical parameters
Thermodynamic parameters
Antimicrobial activities

ABSTRACT

A novel series of metal complexes with 4-(2,3-dimethyl-1-phenylpyrazol-5-one azo)-3-aminophenol ligand (HL) are prepared and characterized by elemental analyses, IR, UV–Visible spectra, ^{1}H NMR spectra, mass spectra, X-ray diffraction analysis, conductivity measurements and magnetic susceptibility measurements as well as thermal analysis. The IR spectrum revealed that the ligand (HL) coordinates as monobasic tridentate manner with ONO donor sites of nitrogen atom of azo group (—N═N), oxygen atom of the deprotonated phenolic —OH group and exocyclic carbonyl oxygen atom forming a five/six-membered chelate structures. The ^{1}H NMR spectra data indicated that the phenolic proton is also displaced during complexation. From the magnetic and spectral studies, it was obvious that the geometrical structures of these complexes are octahedral. The molecular structures of the ligand (HL) and its metal complexes are optimized theoretically and the quantum chemical parameters are calculated. The XRD patterns of the ligand (HL) and complex **(3)** are a mixture of crystalline and amorphous phases. The activation thermodynamic parameters, such as activation energy (E_a), enthalpy (ΔH^*), entropy (ΔS^*), and Gibbs free energy change of the decomposition (ΔG^*) are calculated using Coats–Redfern and Horowitz–Metzger methods. The ligand (HL) and its metal complexes are screened for their antimicrobial activity against, four bacteria (two Gram positive, i.e. *Bacillus subtilis*, *Streptococcus pneumoniae*, and two Gram negative, i.e. *Escherichia coli* and *Pseudomonas aeruginosa*) and two fungi species (*Aspergillus fumigatus* and *Candida albicans*). The obtained data implies that all the complexes have high antimicrobial activities toward *B. subtilis*, *S. pneumoniae*, *E. coli* and *A. fumigatus* than the ligand (HL). In addition to that, complexes **(1)**, **(3)** and **(5)** showed antifungal effect against *C. albicans*.

1. Introduction

Many authors reveal an excellent work devoted to the synthesis and characterization of azodyes as well as their metal complexes [1–4]. The variety of coordination modes of azodye of 3-aminophenol and/or pyrazolone were demonstrated in a number of complexes and their biological applications as well and potentiometric studies have been of considerable interest [5–7]. Many attempts were done to prepare symmetric/asymmetric polydentate ligands in order to achieve rare coordination number with divalent metal ions whose importance was mainly due to their ability to form metal chelates. Due to new interesting applications found in the field of pesticides and medicine, the metal complexes with bi/tridentate O, N/O, N, O types of alternative structures had attracted the attention of chemists [8]. Azo compounds are known to be involved in a number of biological reactions which based on heterocyclic amines have higher strength and give brighter dyeing than those derived from aniline-based diazo components [9]. Furthermore, they were proved to have biological activity against bacteria and fungi organisms [10,11]. Azo derivatives containing antipyrine moiety have many advantages including color depending effect as an intrinsic property leading to better dye ability.

The data from our laboratory [1,12–14] have demonstrated that the bidentate azodye ligands play a key role in making new complexes with transition metal ions. However, little is known concerning the constitution of these complexes, as well as the chemistry involved in their preparation, or the structural and coordination in such complexes. El-Sonbati et al. [11,15] found that the stability of multiple hydrogen bonded ligands depends not only on the number of hydrogen bonds but also on the hydrogen bonding pattern.

This paper describes the characterization of 4-(2,3-dimethyl-1-phenylpyrazol-5-one azo)-3-aminophenol ligand (HL) and its metal complexes by elemental analyses, IR, ^{1}H NMR, UV–Vis spectra, X-ray diffractometer, magnetic moment, molar conductance, and thermal analysis. The antimicrobial activity of the ligand (HL) and its metal complexes are studied and comparison of the antimicrobial activity results of the ligand (HL) and its metal complexes with the standard antibacterial and

* Corresponding author.
E-mail address: elsonbatisch@yahoo.com (A.Z. El-Sonbati).

http://dx.doi.org/10.1016/j.molliq.2016.02.026
0167-7322/

antifungal drugs was carried out. The molecular structures of the investigated ligand (HL) and its metal complexes were studied and quantum chemical parameters were calculated. Moreover, the thermodynamic parameters are calculated and discussed.

2. Experimental

2.1. Preparation of the ligand (HL)

The ligand (HL) was prepared as described previously [5,7] by coupling an equimolar amount of 1-phenyl-2,3-dimethyl-4-aminopyrazol-5-one and 3-aminophenol as shown in Fig. 1. In a typical preparation, 25 ml of distilled water containing 0.01 mol hydrochloric acid was added to 1-phenyl-2,3-dimethyl-4-aminopyrazol-5-one (0.01 mol). To the resulting stirred and cooled (0 °C) mixture, a solution of 0.01 mol sodium nitrite in 20 ml of water was added dropwise. The formed diazonium chloride was consecutively coupled with an alkaline solution of 0.01 mol 3-aminophenol, in 10 ml of pyridine. Immediately, the deep purple precipitate formed was filtered through sintered glass crucible and washed several times by distilled water. The crude product was purified by recrystallization from hot ethanol (yield ~68%) then dried in a vacuum desiccator over anhydrous P_2O_5. The structure of the formed ligand (HL) was established by elemental analyses, IR and ^{1}H NMR spectroscopies.

2.2. Preparation of complexes

The metal complexes were prepared by the addition of hot solution (60 °C) of the appropriate metal chloride (0.664 mmol) in absolute ethanol (15 ml) to the hot solution (60 °C) of the organic ligand (0.3 g HL)

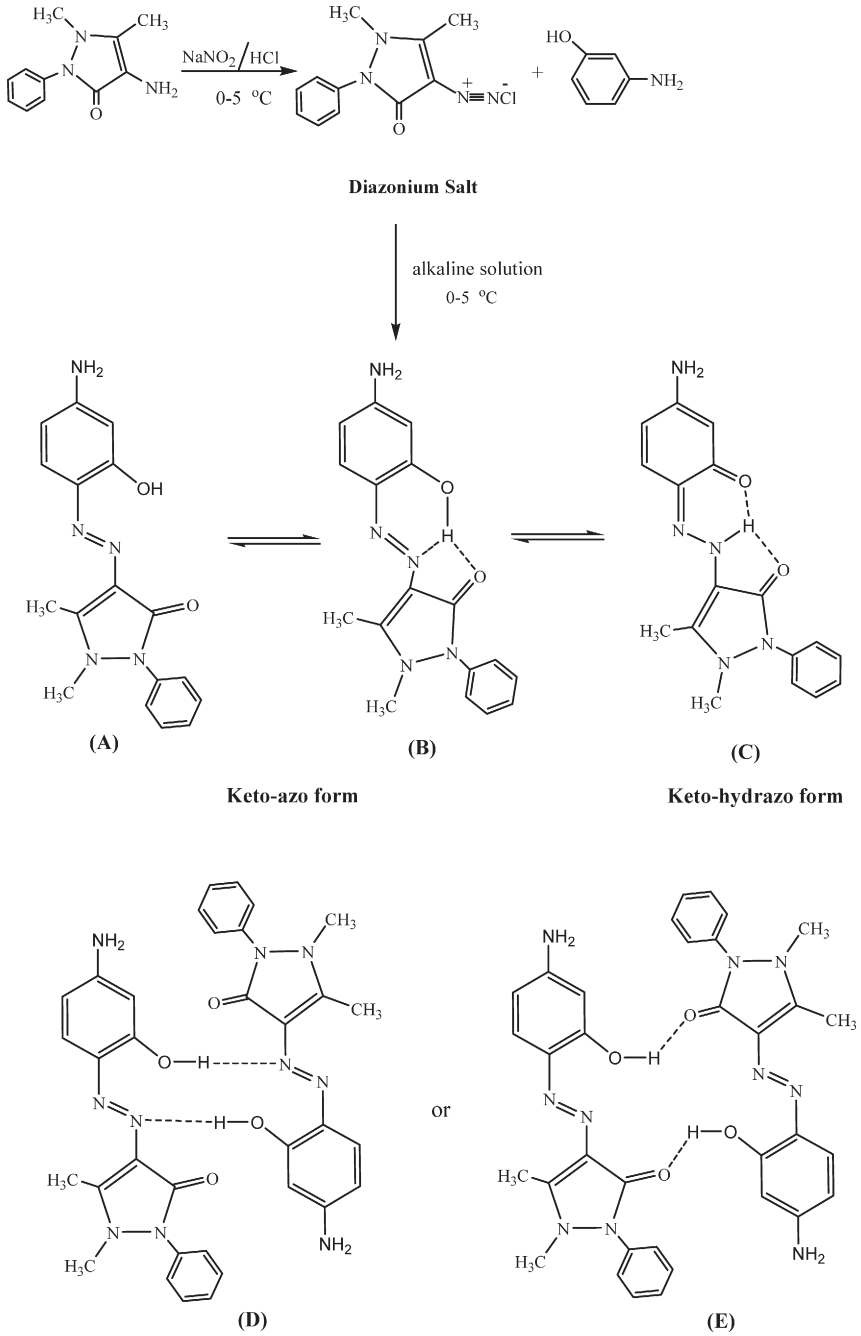

Fig. 1. The formation mechanism and tautomeric structures of the azo ligand (HL).

Table 1
Elemental analyses data physical properties of HL ligand and its complexes.

Compound	Color (% yield)	M.p. (°C)	Exp. (calcd.)%				μ_{eff} (B.M.)	A_m (Ω^{-1} mol^{-1} cm^2)
			C	H	N	M		
HL ($C_{17}H_{17}N_5O_2$)	Reddish brown (68)	265	63.09 (63.16)	5.25 (5.26)	21.65 (21.67)	–	–	–
[Cr(L)Cl_2H_2O] H_2O **(1)** ($C_{17}H_{20}N_5O_7Cl_2Cr$)	Green (83)	>300	42.78 (42.42)	3.90 (3.74)	14.70 (14.56)	10.41 (10.79)	4.2	58.0
[Co(L)Cl$(H_2O)_2$] .5H_2O **(2)** ($C_{17}H_{30}N_5O_7ClCo$)	Black (94)	>300	37.54 (37.61)	3.55 (3.69)	12.92 (12.90)	10.64 (10.86)	4.3	57.0
[Ni(L)Cl$(H_2O)_2$] 5H_2O **(3)** ($C_{17}H_{30}N_5O_7ClNi$)	Green (80)	>300	37.42 (37.63)	3.90 (3.69)	12.86 (12.91)	10.62 (10.82)	3.1	34.0
[Cu(L)Cl$(H_2O)_2$] 3H_2O **(4)** ($C_{17}H_{26}N_5O_7ClCu$)	Brown (70)	>300	39.60 (39.92)	3.60 (3.91)	13.69 (13.70)	12.62 (12.42)	1.8	30.0
[Cd(L)Cl$(H_2O)_2$]H_2O **(5)** ($C_{17}H_{22}N_5O_7ClCd$)	Yellowish brown (75)	>300	38.45 (38.94)	3. 89 (3.82)	13.74 (13.36)	21.45 (21.46)	d[a]	55.0

[a] d = diamagnetic.

in ethanol and DMF (15 ml). The resulting mixture was heated with stirring to evaporate all the solvents to get a precipitate. The precipitate was dried and weighed to calculate the percent yield. All the above steps were repeated for all the selected d-transition metals. The elemental analyses data and physical properties are listed in Table 1.

2.3. Methodology of antimicrobial

The ligand (HL) and its metal complexes **(1–5)** of 5 mg/ml concentration were tested for their antibacterial and antifungal activities. These assays were performed at the Regional Center for Mycology and Biotechnology, Al-Azhar University, Egypt. The tested compounds were evaluated against two Gram positive bacteria (*Bacillus subtilis* (RCMB 010067) and *Streptococcus pneumoniae* (RCMB 010010)), two Gram negative bacteria (*Escherichia coli* (RCMB 010052) and *Pseudomonas aeruginosa* (RCMB 010043)) and two fungal species (*Aspergillus fumigatus* (RCMB 02568) and *Candida albicans* (RCMB 05036)) [16]. Well diameters (6 mm) were made in the media and the hole was loaded with the compounds. Amphotericin B was taken as a reference for the antifungal effect, while ampicillin was used as standard for the evaluation of antibacterial activity against Gram positive bacteria and gentamicin was used as a standard in assessing the activity of the tested compounds against Gram negative bacteria [16]. The results are expressed as the mean of zone of inhibition in mm ± standard deviation. Optical densities of antimicrobial were measured after 24 h at 37 °C to bacteria organisms and measured after 48 h at 28 °C to fungal species. The plates were then incubated at 37 °C or 28 °C for bacteria and fungi, respectively. The diameters of inhibition zone were determined after 24 h and 3–5 days for bacteria and fungi, respectively, taking the consideration of the control.

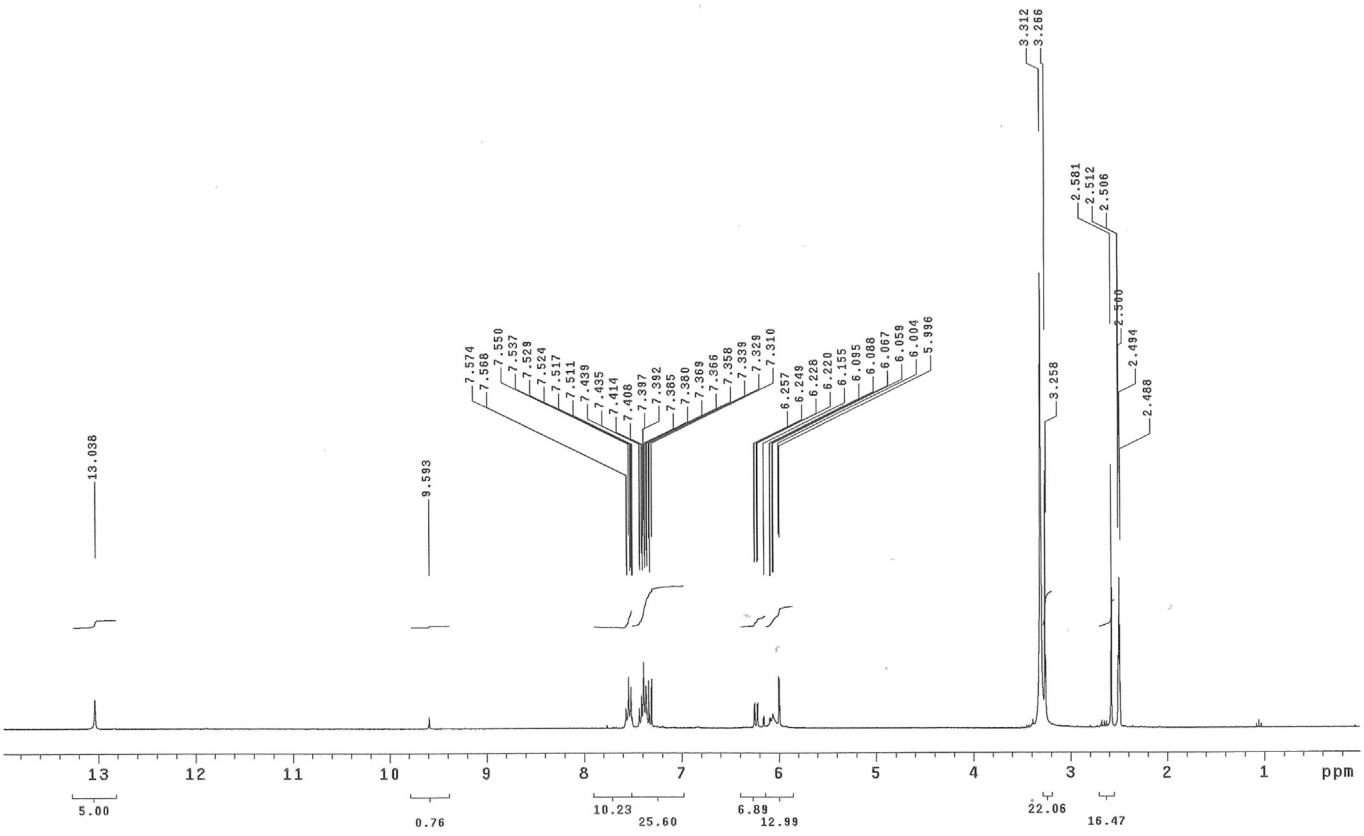

Fig. 2. ^{1}H NMR spectrum of HL ligand.

2.4. Measurements

All the compounds and solvents used were purchased from Aldrich and Sigma and used as received without further purification. Elemental microanalyses of the separated ligand and solid chelates for C, H, and N were determined on Automatic Analyzer CHNS Vario ELIII, Germany. Mass spectra were recorded by the EI technique at 70 eV using MS-5988 GS-MS Hewlett-Packard. The IR spectra were recorded as KBr disks using a Perkin-Elmer 1340 spectrophotometer. The ^{1}H NMR spectrum was obtained with a JEOL FX90 Fourier transform spectrometer with DMSO-d_6 as the solvent and TMS as an internal reference. X-ray diffraction analysis of the compounds in powder form was recorded on an X-ray diffractometer in the range of diffraction angle $2\theta^o = 5–60^o$. This analysis was carried out using CuKα radiation ($\lambda = 1.54056$ Å). The applied voltage and the tube current are 40 KV and 25 mA, respectively. Ultraviolet–visible (UV–Vis) spectra of the compounds were recorded in Nujol mulls using a Unicom SP 8800 spectrophotometer. The magnetic moment of the prepared solid complexes was determined at room temperature using the Gouy's method. Mercury(II) (tetrathiocyanato)cobalt(II), [Hg{Co(SCN)$_4$}], was used for the calibration of the Gouy tubes. Diamagnetic corrections were calculated from the values given by Selwood [17] and Pascal's constants. Magnetic moments were calculated using the equation, $\mu_{eff.} = 2.84\,[T\chi_{M\ coor.}]^{1/2}$. Thermal studies were computed on Simultaneous Thermal Analyzer (STA) 6000 system using thermogravimetric analysis (TGA) method. Thermal properties of the samples were analyzed in the temperature range from 30 to 1000 °C at the heating rate of 10 °C/min under dynamic nitrogen atmosphere. ESR measurements of powdered samples were recorded at room temperature using an X-band spectrometer utilizing a 100 kHz magnetic field modulation with diphenyl picrylhydrazyl (DPPH) as a reference material. The conductance measurement was achieved using Sargent Welch scientific Co., Skokie, IL, USA. The molecular structure of the investigated compound was optimized initially with the PM3 semiempirical method so as to speed up the calculations. The resulting optimized structures were fully re-optimized using ab initio Hartree–Fock (HF) [18] with 6-31G basis set. The molecules were built with the Gauss View 3.09 and optimized using Gaussian 03W program [5,19]. The corresponding geometries were optimized without any geometry constraints for full geometry optimizations. Frequency calculation was executed successfully, and no imaginary frequency was found, indicating minimal energy structures.

2.5. Methods of calculations

The molecular geometry for the tested compound was fully optimized using Density functional theory B3LYP method, where (B3) [20,21] stands for Becke's three parameter exact exchange-functional combined with gradient-corrected correlation functional of Lee, Yang and Parr (LYP) [22] by implementing 6–311 + g(d,p) [23] and LANL2DZ [24,25] as basis sets for the isolated ligand and complex, respectively. All the calculations were done using the Gaussian 09 software package [26]. The optimized structures were visualized using Chemcraft version 1.6 package [5] and GaussView version 5.0.9 [27]. As a consequence of using multiplicity other than singlet, both HOMO and LUMO split into two levels with different spins namely, "Alpha" (α) and "Beta" (β) were employed. The energy difference, ΔE is measured as the smallest difference between LUMO and HOMO having the same spin since using different spins produce an optically spin forbidden transition (dark excited state). The binding energy of metal to all moieties in the complex was calculated by subtracting the total energy of the complex from the summation of the energies of isolated metal ion and (single point at the optimized geometry of the complex excluding the metal ion) using LANL2DZ [24,25] as a basis set.

3. Results and discussion

3.1. Characterization of the ligand (HL)

Our earlier studies on coordination behavior of azodye derivatives have shown that this 4-(2,3-dimethyl-1-phenylpyrazol-5-one azo)-3-aminophenol ligand (HL) (Fig. 1) presents a variety of chelating coordination behavior, depending on the nature of the metal ion and ligand.

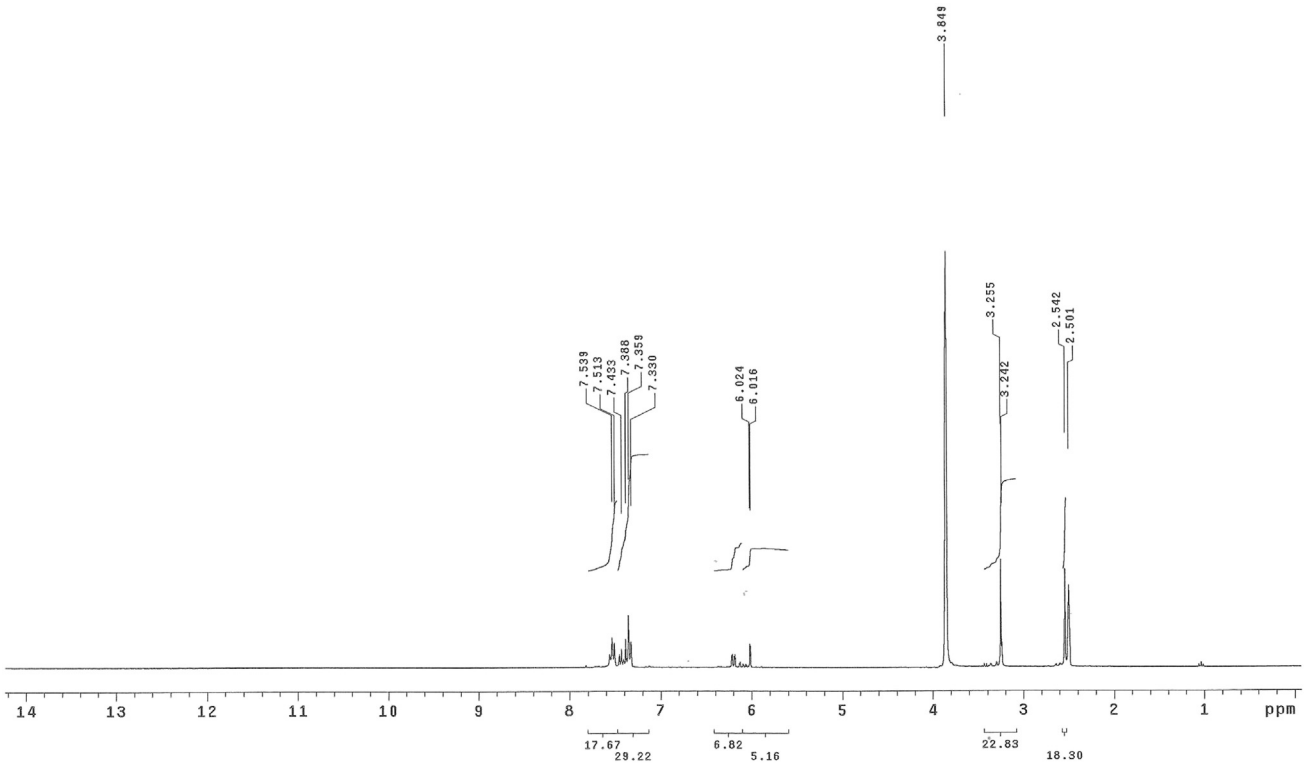

Fig. 3. ^{1}H NMR spectrum of HL ligand with D_2O.

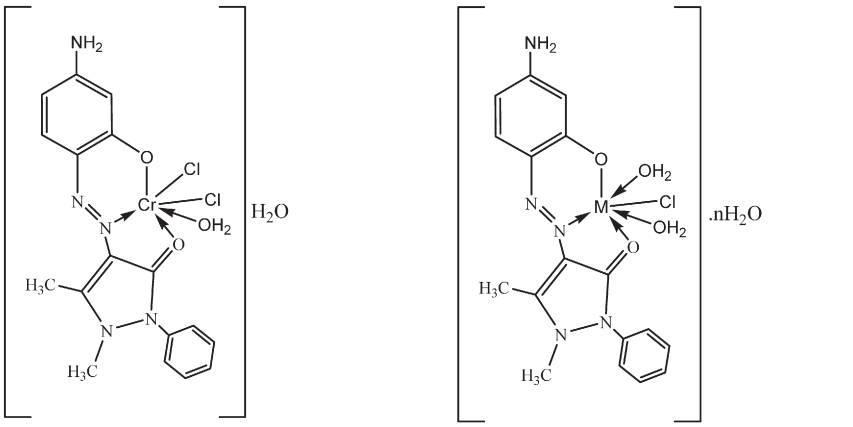

Fig. 4. The structure of complexes (1–5).

Structure of the ligand was established by UV, IR and ^{1}H NMR spectral data in addition to the elemental analysis data. A basic structure requirement for tautomerism is the presence of a proton in the molecule. This requirement is manifested in case of azodye containing an —OH group conjugated with the azo group and these dyes exist as a tautomeric azo-hydrazo mixture both in solution and in the solid phase [28]. Thus the ligand under investigation is also capable of exhibiting keto-azo (Fig. 1A) and keto-hydrazo tautomerisms (Fig. 1C). It has been reported that the azo ligand exhibited a strong band in the range 37,000–35,200 cm^{-1}, whereas hydrazones exhibited a strong band above 31,250 cm^{-1} in ethanol medium [29]. However, the ultraviolet spectrum of the ligand under investigation gave characteristic band at ~35,500 cm^{-1} (in ethanol) for the azo form. In addition to this, the spectrum showed an absorption band at 21,930 cm^{-1} due to π–π* electronic transition involving the whole conjugate system (five-membered oxygen heterocycles and the azo group) [30].

In agreement with spectrum data, infrared spectrum of HL ligand gives interesting results and conclusions. The formation of ligand is confirmed by the absence of the NH_2 group of 4-amino-1-phenyl-2,3-dimethylpyrazolin-5-one and instead a strong new band appeared at ~1490 cm^{-1} corresponding to the azo dye (N═N) group (Fig. 1) [8] was reported. Additionally, IR spectrum of the HL ligand shows a broad band assigned to phenolic OH group; υ(OH) [5,7] and a strong band at 1323 cm^{-1} assigned to the stretching frequency of the phenolic C—O bond; υ(C—O) [11], which affected on complexation with different degrees. The bands appearing in the region 1480 and 750 cm^{-1} were usual modes of phenyl ring vibration [11], while a band at 2848 cm^{-1} for CH_3 stretching vibrations of methyl group was found [8].

Hydrogen bonding represents one of the most versatile interactions that could be used for molecular recognition. It might be possible to tune the strength of the hydrogen bond effectively by linking the hydrogen-bonding site to a reaction center through a conjugated spacer,

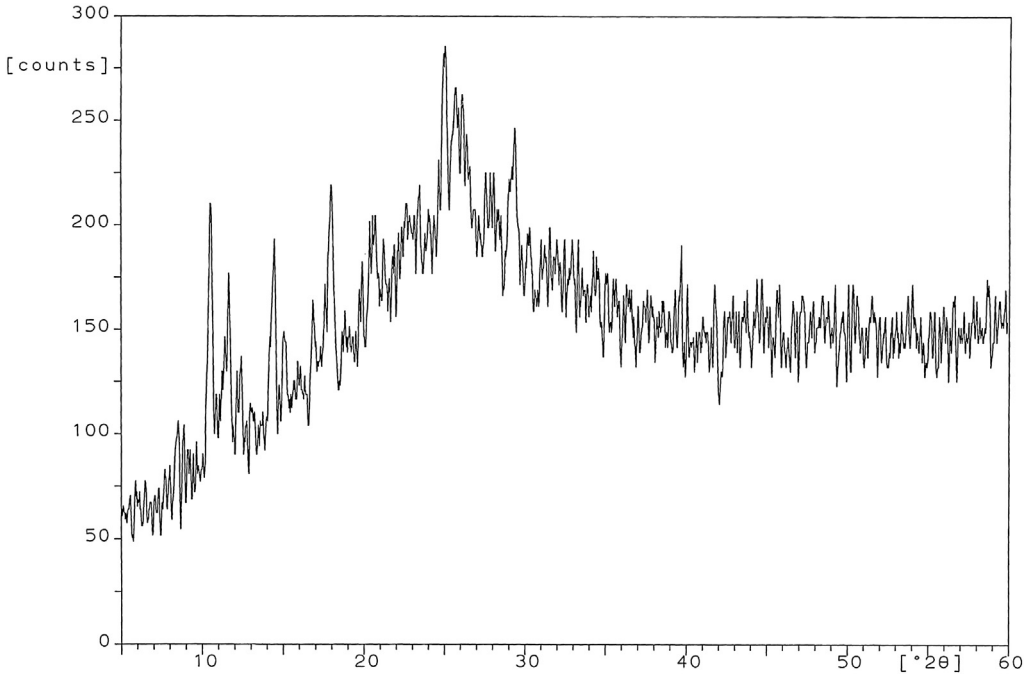

Fig. 5. X-ray diffraction pattern of HL powder form.

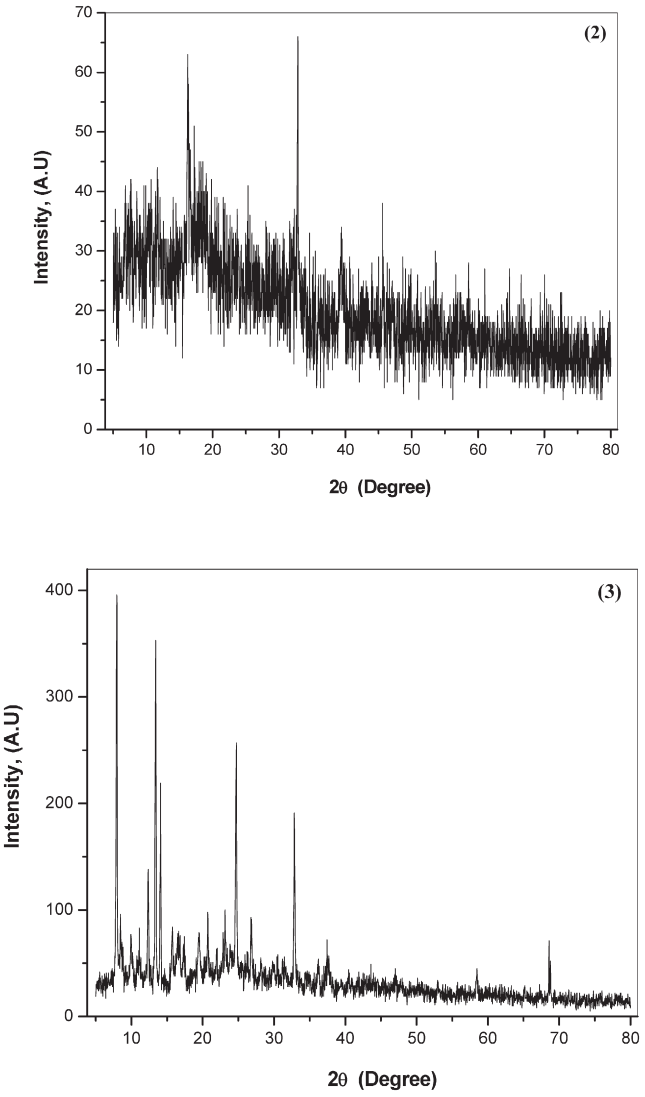

Fig. 6. X-ray diffraction patterns for complexes (2) and (3).

and by altering the charge state of the reaction center in the solution. At the hydrogen-bonding end, azodye is used as a proton acceptor to form a hydrogen bond with OH group of ligand.

El-Sonbati et al. [8,13–15] found that three types of hydrogen bonds may exist in equilibrium with each other. The hydrogen bond in this case is of intramolecular type either with (B) OH…N═N and OH…O(antipyrine) or (C) NH…O(antipyrine) and NH…O(amino phenol) as shown in Fig. 1. The predominant hydrogen bond is probably of the first/second type due to the formation of a chelate structure. Intermolecular hydrogen bonding can form a cyclic dimer through the (D) O—H—N═N type between OH/N═N of one molecule and OH/N═N group of another one, (E) O—H—O═C type between OH/C═O(antipyrine) of one molecule and OH/C═O(antipyrine) group of another one as shown in Fig. 1.

In general, hydrogen bonding involving OH group is a proton donor and their O atoms are proton acceptors. Both intra and intermolecular OH…N may form a number of structures in a simultaneous equilibrium.

^{1}H NMR spectrum of the ligand was recorded in DMSO-d_6 at room temperature which supports the occurrence of the form depicted in Figs. 2 and 3. In ^{1}H NMR spectrum of the ligand, the ═C—CH_3 and —N—CH_3 protons were observed as singlet at δ 2.47 and 2.60 ppm, respectively. In the aromatic region, a few doublets and in few cases some overlapping doublets/multiplets are observed in the range of δ 6.10–7.6 ppm. Another singlet corresponding to one proton for azodye free ligand is observed in the range of δ ~ 9.59 and 13.03 ppm. This signal disappeared when a D_2O exchange experiment was carried out. It can be assigned to OH and/or NH (Fig. 1). Absence of —CH (~3.85 ppm) proton signal of the ligand (HL) moiety indicated the existence of the ligand in the keto-azo form. According to El-Sonbati et al. [8], hydrogen bonding leads to a large deshielding of the protons.

3.2. Structure of the metal complexes

By comparing the infrared spectrum of the ligand and its complexes the following features for some of the prepared complexes are observed:

1. In IR spectra of all complexes, υ(C═O) for the exocyclic carbonyl group at 1620 cm^{-1} is shifted, with 15–25 cm^{-1}, to lower wave numbers. This indicates that the exocyclic carbonyl oxygen is bonded to metallic ions [31].
2. The N═N stretching frequency of the azo group is shifted to lower frequency by ~25 cm^{-1} due to the involvement of one of the azo nitrogen atoms in coordination with metal ion [8]. This lowering of frequency can be explained by the transfer of electrons from the nitrogen atom to the metal ion due to coordination.
3. A medium intensity broad band at 2935 cm^{-1} in the spectrum of ligand is due to υ(OH) stretching vibration [5]. The band at 1275 cm^{-1} is characteristic for phenolic υ(C—O) and it shifted to 1260–1235 cm^{-1} in all the complexes, confirms the chelation of phenolic oxygen to metal ions.
4. Based on the above spectral evidences, it is concluded that the ligand is coordinated to the metal ions as a monobasic tridentate chelating agents, coordinated to the metal ions *via* the azodye nitrogen, proton displacement from the phenolic OH group, i.e. M—O bonding is

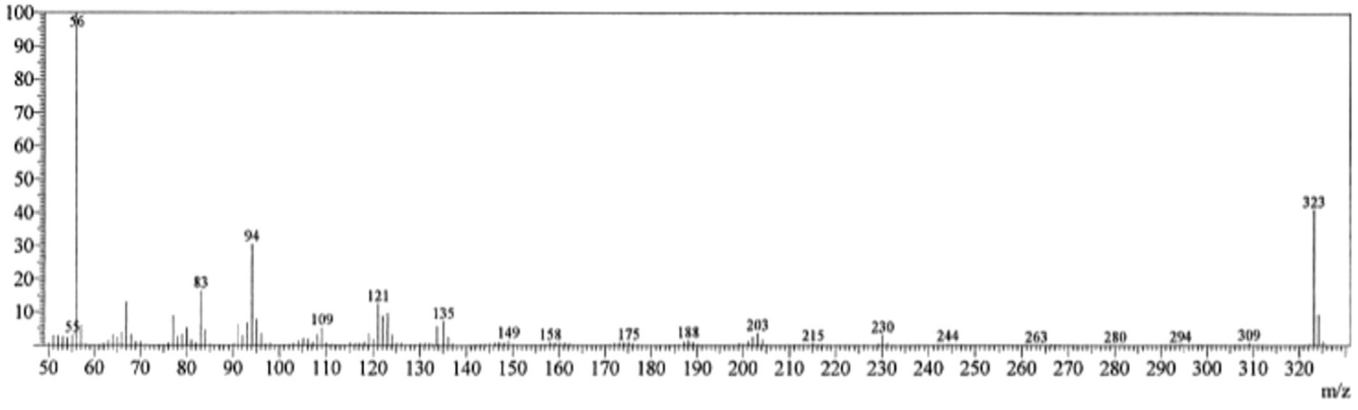

Fig. 7. Mass spectrum of HL ligand.

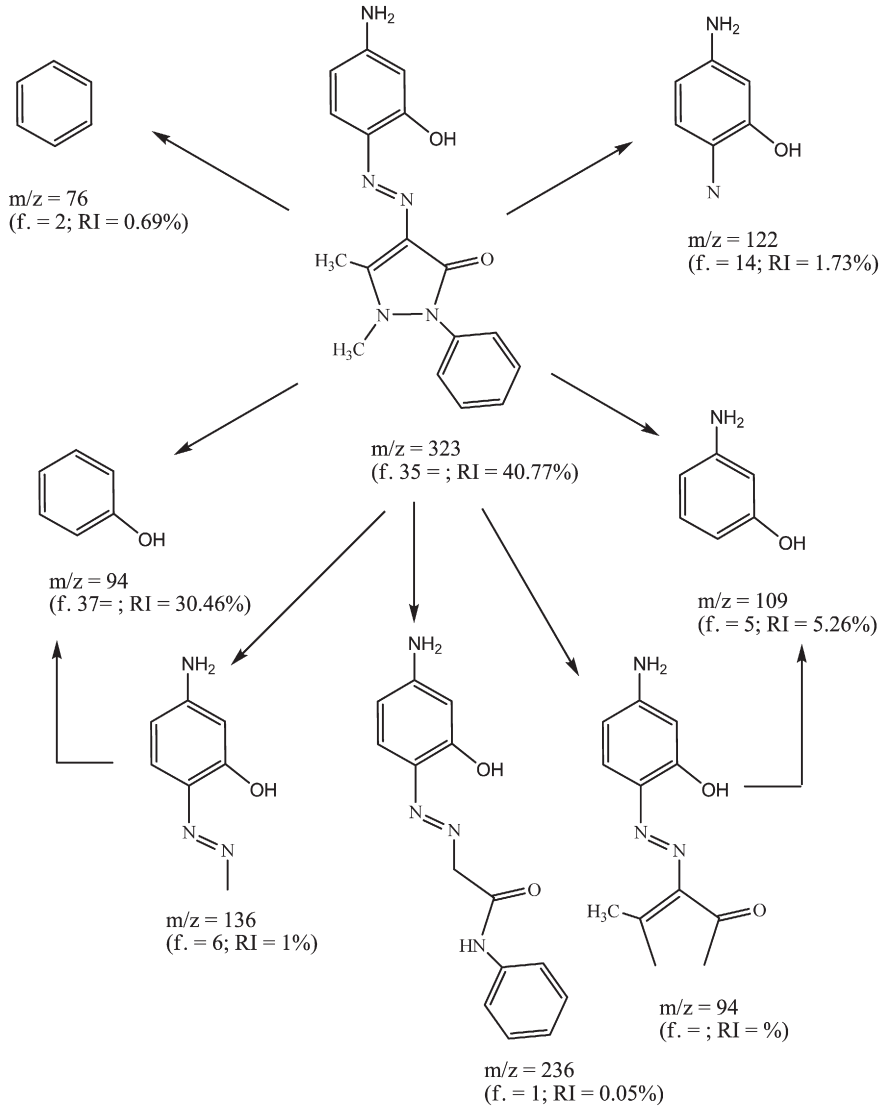

Scheme 1. Fragmentation patterns of HL ligand.

identified and exocyclic carbonyl oxygen atoms forming the more stable six membered chelate rings (Fig. 4).

5. Far infrared spectra of the metal complexes showed several non-ligand bands of low intensity appearing in the regions 505–595 and 415–455 cm^{-1} which can be assigned to υ(M—O) and υ(M—N) vibrations, respectively [8].
6. The existence of the broad band in the region 3440–3455 cm^{-1} in all the complexes confirms the O—H stretching of the coordinated and

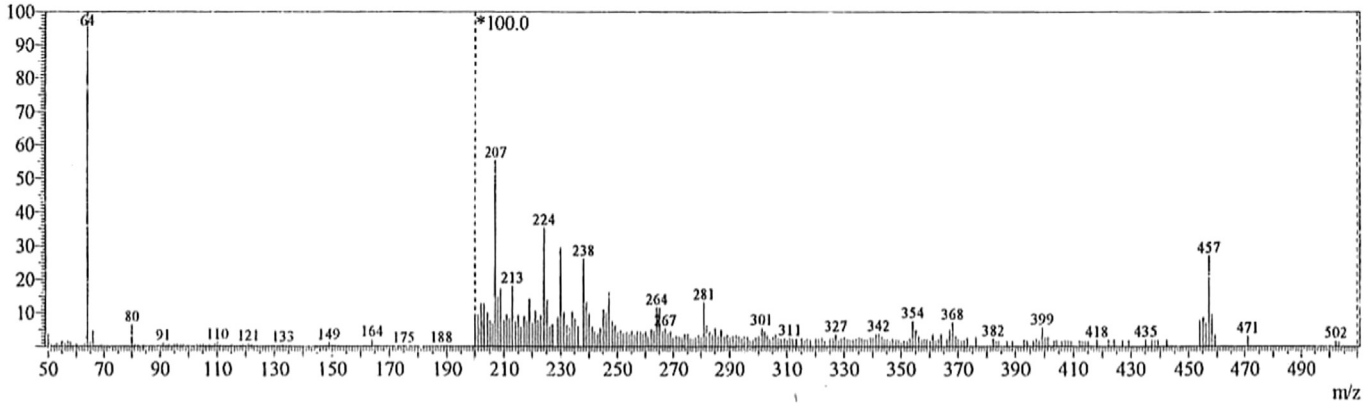

Fig. 8. Mass spectrum of complex (5).

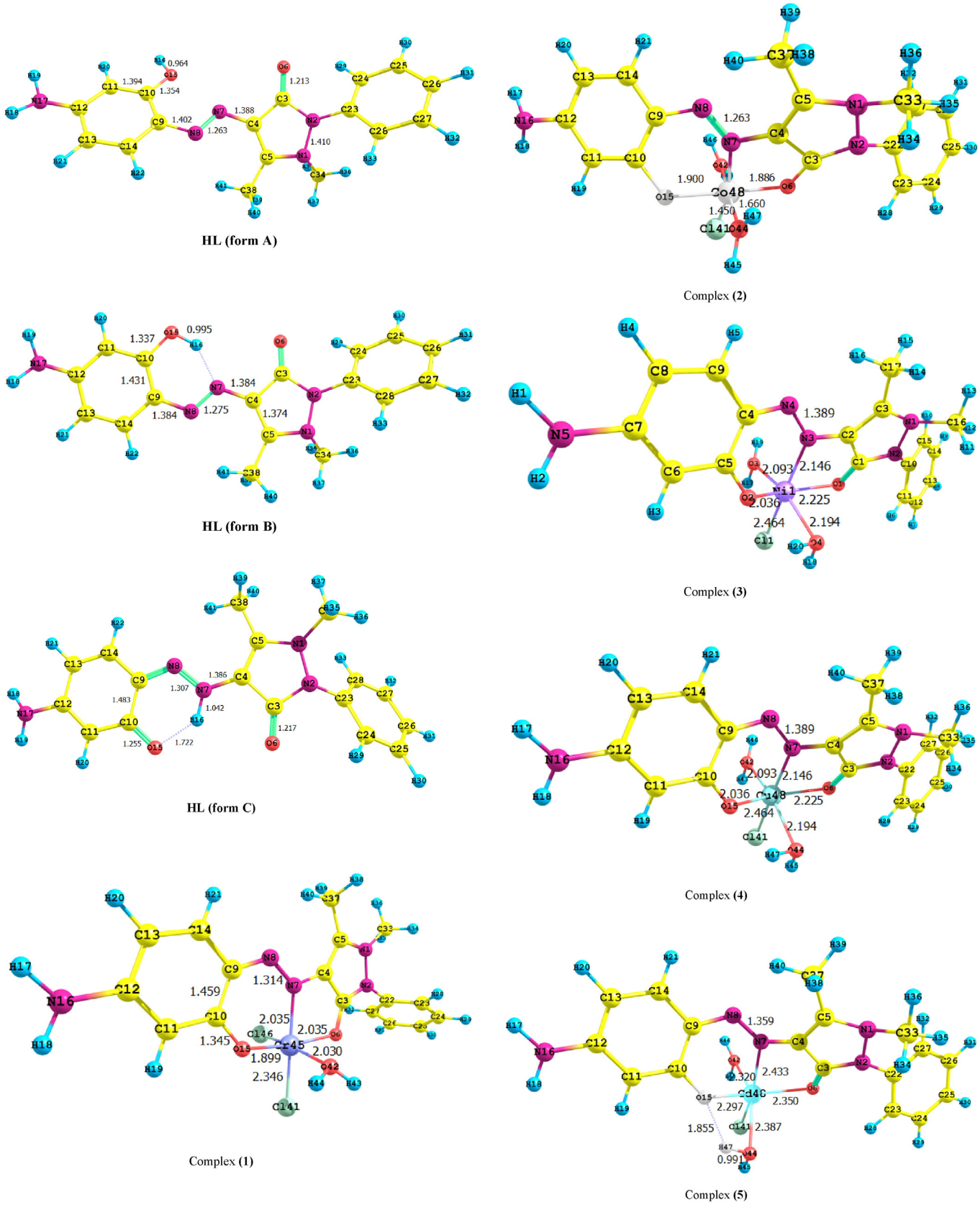

Fig. 9. The optimized structure of HL ligand and its metal complexes within numbering of atoms.

hydration water molecules. Also, according to Stefov et al. [32], coordinated water should exhibit frequencies and appear in the spectra of metal complexes at 870, 580 and 500 cm^{-1}.

^1H NMR spectrum of cadmium(II) complex recorded in DMSO-d_6 further substantiates the mode of coordination suggested by IR spectral studies. In the spectrum of cadmium(II) complex, the proton signal due

to —OH disappears and this is a clear indication that phenolic oxygen is bonded to the metal ion after deprotonation. Signals for N—CH_3 and —CH_3 protons do not show any significant changes when compared to the free ligand. Thus, from IR and ^{1}H NMR spectral data it is clear that the ligand is bonded to the metal ion in a keto-azo form.

3.3. X-ray diffraction analysis

The X-ray diffraction, XRD, patterns of the ligand (HL) and its metal complexes **(2)** and **(3)** are shown in Figs. 5 and 6. The XRD patterns of the ligand (HL) and complex **(3)** have sharp diffraction peaks at around $2\theta = 10–20^o$ and $2\theta = 25–30^o$, this indicates that HL and complex **(3)** are a mixture of crystalline and amorphous phases. While the XRD pattern of complex **(2)** is amorphous phase.

3.4. Mass spectra

The electron impact mass spectra of ligand and its Cd(II) complex are recorded and investigated at 70 eV of electron energy. It is obvious that, the molecular ion peaks are in good agreement with their suggested empirical formula as indicated from elemental analysis. The mass spectrum fragmentation mode of ligand (HL) shows the exact mass of 323 corresponding to the formula $C_{17}H_{17}N_5O_2$ (Fig. 7). The ion of m/z = 323 undergoes fragmentation to a stable peak at m/z = 122 or 109 or 94 or 76 as shown in Scheme 1. The mass spectrum fragmentation mode of complex **(5)** shows the exact mass of 523 corresponding to the formula $[Cd(L)Cl(H_2O)_2]\,H_2O$ (Fig. 8). The ion of m/z = 502 (M-H_2O) undergoes successive fragmentation to a stable peak at m/z = 64 that may correspond to C_5H_4 molecule. The loss of $C_{11}N_4H_3O$ leads to the fragmentation with m/z = 207. The loss of C_6H_7N molecule leads to the fragmentation with m/z = 91. The loss of $C_{11}N_5H_6O$ molecule leads to the fragmentation with m/z = 224.

3.5. Molecular structures of the ligand and its complexes

Theoretical approaches made by Liang and Lipscomb [33] indicated that the nitrogen atom is more negatively charged than the oxygen atom in the isolated metal ion and consequently it may account for the coordination of the nitrogen atom rather than the oxygen atom, to the metal ion. Moreover, these authors have found that in the presence of the metal ion, the tridentate binding conformation with both N and (O,O) atoms coordinated to the metal ions is favored.

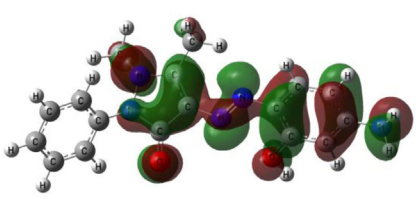

HOMO of HL

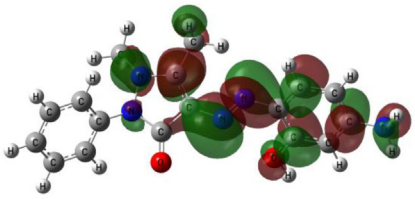

LUMO of HL

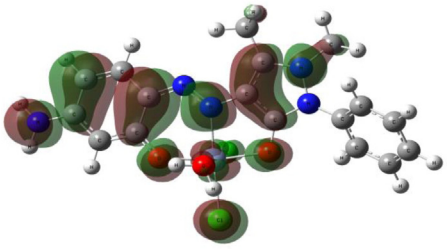

HOMO of alpha electron of complex **(1)**

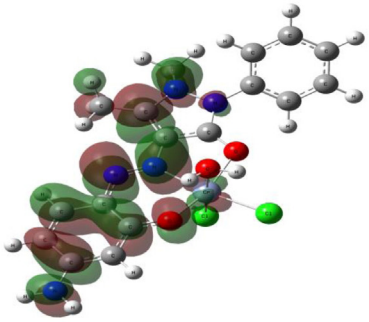

LUMO of alpha electron of complex **(1)**

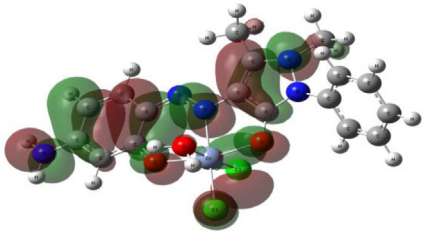

HOMO of beta electron of complex **(1)**

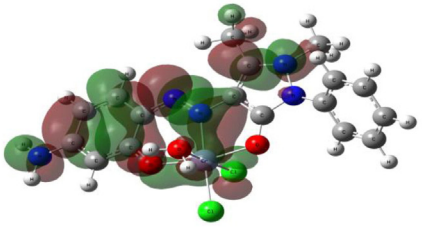

LUMO of beta electron of complex **(1)**

Fig. 10. HOMO and LUMO molecular orbitals of ligand (HL) and its complexes (1–5).

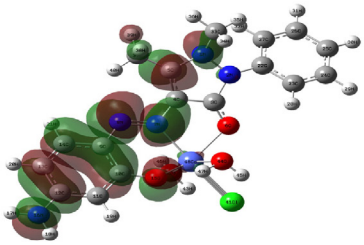

HOMO of alpha electron of complex **(2)**

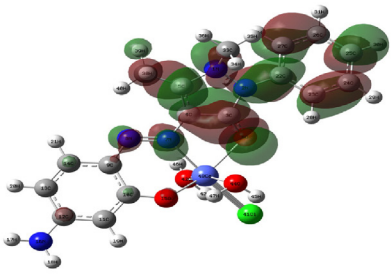

LUMO of alpha electron of complex **(2)**

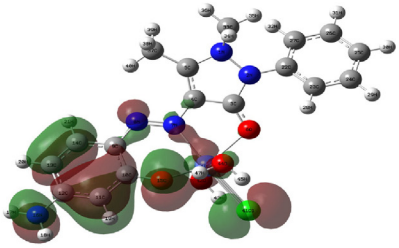

HOMO of beta electron of complex **(2)**

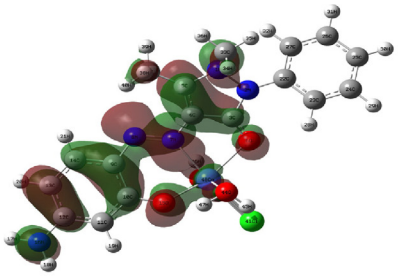

LUMO of beta electron of complex **(2)**

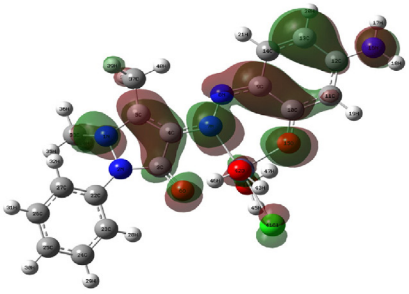

HOMO of alpha electron of complex **(3)**

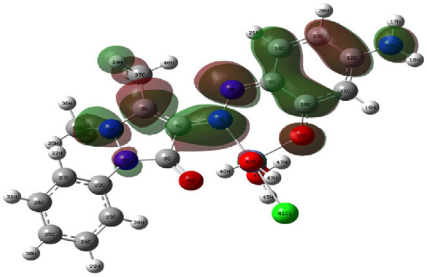

LUMO of alpha electron of complex **(3)**

Fig. 10 (*continued*).

The optimized structures of the ligand (HL) and its metal complexes are presented in Fig. 9. Selected geometric parameters such as bond lengths and bond angles of HL ligand and its metal complexes are tabulated in Tables S1–S7 in the supplementary. The HOMO and LUMO states of the HL ligand and its metal complexes are shown in Fig. 10. Quantum chemical parameters of the HL ligand and its metal complexes are obtained from calculations such as energies of the highest occupied molecular orbital (E_{HOMO}) and the lowest unoccupied molecular orbital (E_{LUMO}) as listed in Tables 2 and 3. The total dipole moment in Debye (D) and Total energy (T.E.) in atomic units (a.u.) for all the complexes is shown in Table 3. Higher dipole moment usually signifies a higher possibility to dissolve in polar solvents. Complex **(4)** showed the highest dipole moment, on the other hand, complex **(1)** possesses the lowest dipole moment. The energies of the highest occupied molecular orbital (HOMO), lowest unoccupied molecular orbital (LUMO) with different symmetries α, β and their energy difference, ΔE in a.u. are tabulated in Table 3. Since, the energy difference, ΔE is inversely proportional to the reactivity of the complex, the reactivity of the studied complexes follows the ascending order complex **(1)** < complex **(4)** < complex **(3)** < complex **(5)** < complex **(2)**. The total energy usually is basis set as well as method dependent that usually indicated that their absolute values for energies are almost meaningless. On the other hand, the total energy difference between the complex and its fragments can be used to express the binding energy with acceptable accuracy. The binding energies of the trivalent Cr(III) (complex **(1)**) are more than all divalent metals, which is expected due to more charged metals which create stronger bonds. Furthermore, the divalent metal complexes showed binding energies in the ascending order complex **(5)** < complex **(2)** < complex **(3)** < complex **(4)**.

3.6. Electronic spectra and magnetic moments

The electronic absorption spectra of metal complexes can be classified into three types of spectra depending on the nature of the electronic transitions involved. These types are: (i) spectra associated with electronic transitions within the molecular orbitals of the ligand molecules (L–L spectra), (ii) spectra associated with the metal influenced by the presence of the ligand and these spectra are generally referred to as d-d spectra or crystal field spectra, (iii) spectra involving electronic transition from an orbital lying on the ligand to an orbital lying on the metal or vice versa. Such charge transfer processes are termed ligand to metal (LMCT) charge transfer or metal to ligand (MLCT) charge transfer.

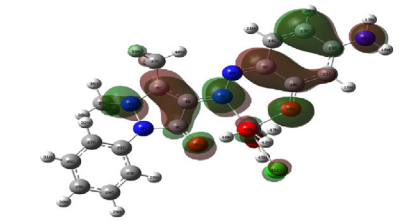

HOMO of beta electron of complex **(3)**

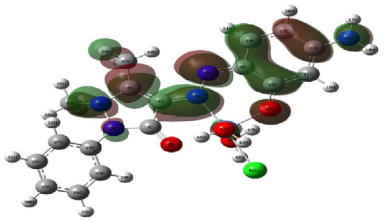

LUMO of beta electron of complex **(3)**

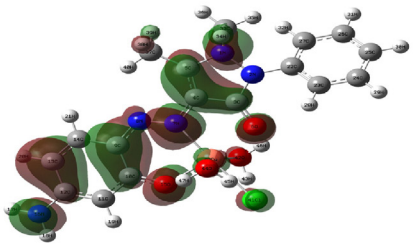

HOMO of alpha electron of complex **(4)**

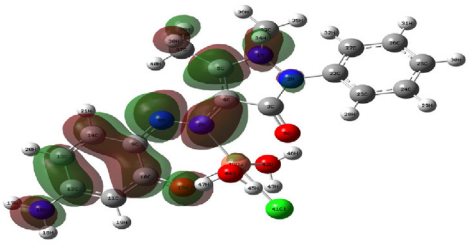

LUMO of alpha electron of complex **(4)**

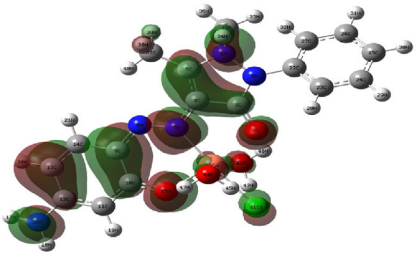

HOMO of beta electron of complex **(4)**

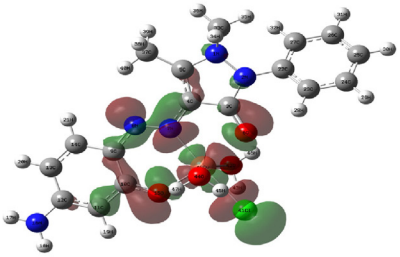

LUMO of beta electron of complex **(4)**

Fig. 10 (*continued*).

In this part, the important role played by magnetic and electronic spectra in determining the geometrical structures of the above investigated metal chelates will be elucidated.

The diffused reflectance spectrum of the Cr(III) complex showed three bands at 16,949, 17,857 and 21,030 cm^{-1} assignable to $^4A_{2g}(F) \rightarrow {}^4T_{2g}(F)$, $^4A_{2g}(F) \rightarrow {}^4T_{2g}$ and $^4A_{2g}(F) \rightarrow {}^4T_{2g}(P)$ spin allowed d-d transitions [34]. The magnetic moment value is found to be 4.2 B.M. for Cr(III) complex, which indicates the presence of Cr(III) complex in octahedral structure. The Ni(II) complex reported herein is high spin with a room temperature magnetic moment value of 3.10 B.M.; which is in the normal range observed for octahedral Ni(II) complexes ($\mu_{eff} = 2.9–3.3$ B.M.) [35]. This indicates that the complex of Ni(II) is six coordinate and probably octahedral [36]. Its electronic spectrum, in addition to show the π–π* and n–π* bands of the free ligand, display three bands, in the solid reflectance spectrum at:

$\nu_1 : 16,407\ cm^{-1} : {}^3A_{2g}(F) \rightarrow {}^3T_{2g}(F).$

$\nu_2 : 17,421\ cm^{-1} : {}^3A_{2g} \rightarrow {}^3T_{1g}(F).$

$\nu_3 : 19,083\ cm^{-1} : {}^3A_{2g} \rightarrow {}^3T_{1g}(P).$

The position of these bands confirms the octahedral configuration of the complex [37,38]. The spectrum showed also a band at 37,174 cm^{-1} which may be attributed to (LMCT).

The reflectance spectrum of the Cu(II) chelate consists of a low intensity shoulder band centered at 16,849 cm^{-1}. The ^2E_g and $^2T_{2g}$ states of the octahedral Cu(II) ion (d^9) split under the influence of the tetragonal distortion and the distortion can be such as to cause the three transitions $^2B_{1g} \rightarrow {}^2B_{2g}$ and $^2B_{1g} \rightarrow {}^2E_g$ to remain unresolved in the spectra [39]. It is concluded that, all three transitions lie within the single broad envelope centered at the same range previously mentioned. This assignment is in agreement with the general observation that Cu(II) d–d transitions are normally close in energy [40]. The magnetic moment of 1.8 falls within the range normally observed for octahedral Cu(II) complex [41]. A moderately intense peak observed in the range 37,383 cm^{-1} is due to ligand–metal charge transfer transition [42]. The electronic spectrum of the Co(II) complex gives band at 21,505 cm^{-1} refers to the charge transfer band. The bands observed are assigned to the transitions $^4T_{1g}(F) \rightarrow {}^4T_{2g}(F)$ at 17,346 cm^{-1} and $^4T_{1g}(F) \rightarrow {}^4A_{2g}(F)$ at 18,165 cm^{-1}, suggesting that there is an octahedral geometry around Co(II) ion [35,43,44]. From the position of the bands, the Co(II) chelates is octahedral with largely covalent bonds between the organic ligand and the metal ion [37]. The magnetic susceptibility measurements lie in the 4.3 B.M. range (normal range for octahedral Co(II) complexes is 4.3–5.2 B.M.), is an indication of octahedral geometry [45]. The complex of Cd(II) is diamagnetic. In analogy with those described for Cd(II) complexes containing N-O donor Schiff bases [42] and according to the empirical formula of this complex, an octahedral geometry was proposed for the Cd(II) complex.

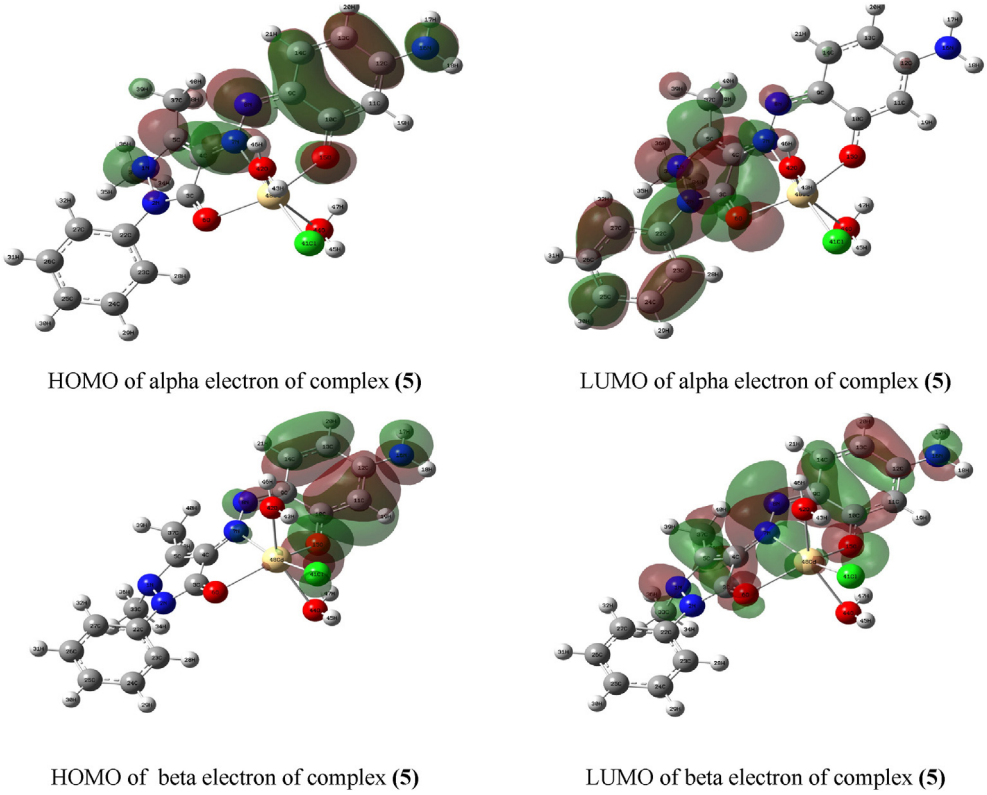

Fig. 10 (*continued*).

3.7. ESR spectrum of Cu(II) complex

The spin-Hamiltonian parameters of copper complexes are listed in Table 4. The spin-Hamiltonian parameters, electronic absorption spectrum and magnetic moment values for the copper(II) complex suggested elongated distorted octahedral Cu(II) complex. Kivelson and Neiman [46] have reported the $g_{||} < 2.3$ for covalent character of the metal–ligand bond and >2.3 for ionic character. Applying this criterion the covalent character of the metal–ligand bond in the complex under study can be predicted. Further, the values are consistent with the mixed Cu—N, and Cu—O bonded copper complexes. The trend $g_{||} > g_{\perp} > g_e$ (2.0023) observed for this complex showed that the unpaired electron is localized in $d_{x2\text{-}y2}$ orbital [47] of the Cu(II) ion and the spectrum features are characteristics of axial symmetry [48]. The unpaired electron in this $3d^9$ case assigned to $3d_{x2\ -\ y2}$ orbital, and the overlapping of this antibonding orbital with the ligand 2 s and 2p σ orbital is often determined by the use of the following equation:

$$\alpha^2 = A_{||}/P_o + (g_{||} - 2.0023) + K_o(g_{\perp} - 2.0023) + 0.04.$$

where α^2 give an approximate indication of the strength of the interaction between the metal and the ligand. P_o is the dipolar contribution to the hyperfine splitting value.

Table 2
The calculated quantum chemical properties for ligand tautomers (A–C).

Compound	E_{HOMO} (a.u.)	E_{LUMO} (a.u.)	ΔE (a.u.)	μ (D)	T.E (a.u)	χ (a.u.)	η (a.u.)	σ $(a.u.)^{-1}$	Pi (a.u.)	S $(a.u.)^{-1}$	Ω (a.u.)	ΔN_{max} (a.u.)
(A)	−0.1973	−0.0689	0.1284	4.529	−1082.473	0.1331	0.0642	15.576	−0.1331	7.788	0.1379	2.073
(B)	−0.2182	−0.1113	0.1069	4.110	−1083.205	0.1648	0.0535	18.702	−0.1648	9.351	0.2539	3.082
(C)	−0.2044	−0.0907	0.1137	6.394	−1082.493	0.1475	0.0568	17.593	−0.1475	8.797	0.1915	2.596

Table 3
The dipole moment, total energy (T.E.), E_{HOMO}, E_{LUMO}, energy difference (ΔE) in a.u., binding energy (B.E.), absolute electronegativities (χ), chemical potentials (Pi), absolute hardness (η), absolute softness (σ), global electrophilicity (Ω), global softness (S) and additional electronic charge (ΔN_{max}) in a.u. of complexes **(1–5)**.

Complex[a]	μ (D)	T.E (a.u.)	E_{HOMO} (a.u.)		E_{LUMO} (a.u.)		ΔE (a.u.)	B.E. (a.u.)	χ (a.u.)	η (a.u.)	σ $(a.u.)^{-1}$	Pi (a.u.)	S $(a.u.)^{-1}$	Ω (a.u.)	ΔN_{max} (a.u.)
			α	β	α	β									
1	7.930	−1335.555	−0.30606	−0.30866	−0.19333	−0.20420	0.10446	−2.345	0.2564	0.0522	19.146	−0.2564	9.573	0.1282	4.909
2	8.892	−1394.419	−0.14284	−0.20361	−0.05179	−0.12976	0.07385	−1.316	0.1667	0.0369	27.082	−0.1667	13.541	0.0833	4.514
3	9.983	−1418.694	−0.18426	−0.18541	−0.09119	−0.09078	0.09307	−1.387	0.1381	0.0473	21.135	−0.1381	10.568	0.0690	2.919
4	10.485	−1445.491	−0.20216	−0.20066	−0.08868	−0.10152	0.09914	−1.397	0.1511	0.0496	20.174	−0.1511	10.087	0.0756	3.048
5	9.326	−1297.389	−0.14674	−0.20420	−0.05343	−0.11494	0.08926	−1.205	0.1596	0.0446	22.407	−0.1596	11.203	0.0798	3.575

[a] Numbers as given in Table 1.

Table 4
The spin Hamilton parameters of Cu(II) complex.

Compound[a]	g_{II}	g_{I}	g_{av}	G	α^2	A_{II}[b]
4	2.221	2.047	2.11	5.5	0.54	94.63

[a] Numbers as given in Table 1.
[b] A values in 10^{-4} cm^{-1}.

In addition there is an exchange coupling interaction between two copper centers explained by Hathaway et al. [49,50] expression $G = (g_{||} - 2)/(g_{\perp} - 2)$. According to Hathaway, if the value of G is greater than four, the exchange interaction is negligible interaction as indicated in solid complex. The calculated G value is given in Table 4 and found to be 5.5. It is clear that $g_{av} > g_{\perp} > 2.04$, characteristic of axial symmetry, suggesting that the principal axes of this structure are parallel to each other and that all the sites are equivalent in every orientation in the static magnetic field. Approximate metal ligand σ -bond coefficient (α^2), which is defined as the fraction of unpaired electron density located on the copper ion, for the present complex fall in the range indicating appreciable in-plane covalency, neglecting the π-bonding with the help of the optical absorption data in the solid state using the relation.

$$g_{av\cdot} = 2.0023 - 4\,\lambda\alpha^2/\Delta E.$$

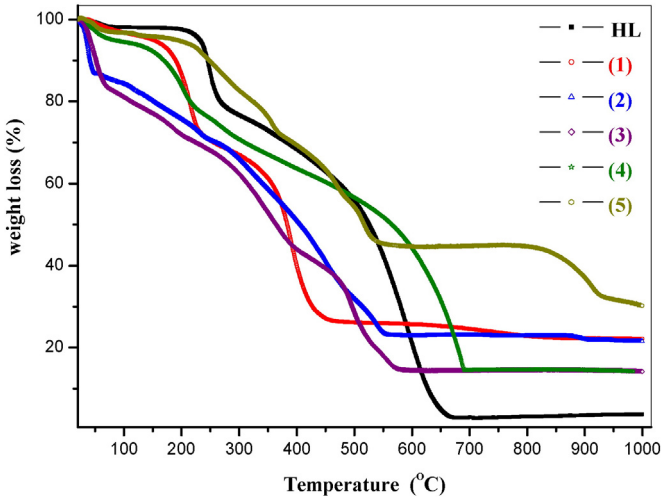

Fig. 11. TGA curves of ligand (HL) and its metal complexes (1–5).

The α^2 value (Table 4) for complex **(4)** indicated considerable covalency in the bonding between the Cu(II) ion and the ligand, comparable to that obtained by El-Sonbati et al. [51,52]. The super-exchange splitting constant $A_{||}$ was obtained semi-empirically, according to Pryce [53].

The small $A_{||}$ value can be attributed to the decreased dipolar interaction. This reduction may be due to the orientation of the 4-(2,3-dimethyl-1-phenylpyrazol-5-one azo)-3-aminophenol groups in a manner so as to increase the separation between successive planes. The $g_{||}/A_{||}$ values showed that the complex has an octahedral geometry [8], and this is further confirmed by the Symons plot [54].

3.8. Thermal analysis

Thermal properties of ligand and its metal complexes were characterized on the basis of thermogravimetric analysis in the temperature range 30–1000 °C as shown in Fig. 11. The temperature intervals and the percentage of loss of masses are listed in Table 5. The ligand showed two decomposition steps. The first stage occurs in the temperature range 50–265 °C which is attributed to loss of C_5H_6 molecule. The second stage in the temperature range 265–1000 °C is corresponding to loss of $C_{12}H_{11}N_5O_2$ molecule.

The TG curve of complex **(1)** showed three decomposition steps, the first step corresponds to the loss of H_2O molecule within the temperature range of 35–125 °C with found mass loss of 4.12% (calcd 3.74%). The second step of decomposition occurs within the temperature range 125–230 °C and corresponds to the loss of H_2O, C_2H_2 and Cl_2 molecules with found mass loss 23.24% (calcd. 23.91%). The third step corresponds to the loss of $C_{12}H_{14}N_5O_{0.5}$ fragment within the temperature range of 230–1000 °C with found mass loss 50.27% (calcd. 49.08%).

The complex **(2)** decomposes in two steps within the temperature range 30–1000 °C. The first step of decomposition within the temperature range 30–45 °C can assigned to the loss of water molecules of hydration with a mass loss 12.44% (calcd. 13.27%). The second step can be attributed to loss of $3H_2O$, HCl and $C_{14}H_{15}N_5O$ fragments with a mass loss of 65.90% (calcd. 66.28%).

The complex **(3)** decomposes in three steps, the first step of decomposition within the temperature range 30–67 °C is due to the loss of $5H_2O$ molecules. The second step of decomposition occurs within the temperature range 67–443 °C and corresponds to the loss of $2H_2O$, HCl and $C_{11}H_{10}O$ molecules with a mass loss 43.74% (calcd. 42.13%). The third step corresponds to the loss of $C_6H_5N_5$ fragment within the temperature range of 443–1000 °C with found mass loss of 26.37% (calcd. 27.11%).

On the other hand, complex **(4)** exhibits three decomposition steps. The first step of decomposition within the temperature range 30–130 °C

Table 5
Weight losses percentage of ligand and its metal complexes[a].

Compound	TG range (°C)	n[a]	Mass loss Calcd. (exp.) %	Total mass loss Calcd. (exp.) %	Assignment	Metallic residue
HL	50–265	1	20.43 (20.30)	100	C_5H_6	
	265–1000	1	79.57 (79.70)	(100)	$C_{12}H_{11}N_5O_2$	–
1	35–125	1	3.74 (4.12)	76.73	H_2O	$0.5Cr_2O_3$
	125–230	1	23.91 (23.24)	(77.63)	$H_2O + C_2H_2 + Cl_2$	+3C
	230–1000	1	49.08 (50.27)		$C_{12}H_{14}N_5O_{0.5}$	
2	30–45	1	13.27 (12.44)	79.55	$4H_2O$	CoO + 3C
	45–1000	1	66.28 (65.90)	(78.34)	$3H_2O + HCL + C_{14}H_{15}N_5O$	
3	30–67	1	16.60 (16.13)	85.84	$5H_2O$	NiO
	67–443	1	42.13 (43.74)	(85.64)	$2H_2O + HCl + C_{11}H_{10}O$	
	443–1000	1	27.11 (26.37)		$C_6H_5N_5$	
4	30–130	1	7.04 (7.30)	84.43	$2H_2O$	CuO
	130–390	1	29.06 (28.70)	(85.15)	$3H_2O + HCl + C_2H_4NO$	
	390–990	1	48.33 (49.15)		$C_{15}H_{11}N_4$	
5	30–129	1	3.44 (3.69)	68.62	H_2O	CdO + 3C
	129–995	1	65.18 (66.16)	(69.85)	$2H_2O + HCl + C_{14}H_{15}N_5O$	

n[a] = number of decomposition steps.
[a] Numbers given in Table 1.

corresponds to the loss of two water molecules of hydration with a mass loss of 7.30% (calcd. 7.04%). The second step of decomposition within the temperature range 130–390 °C corresponds to the loss of $3H_2O$, HCl and C_2H_4NO fragments with a mass loss of 28.70% (calcd. 29.06%). The third step corresponds to the loss of $C_{15}H_{11}N_4$ fragment within the temperature range of 390–990 °C with found mass loss of 49.15% (calcd. 48.15%).

The TG curve of complex **(5)** exhibits two decomposition steps. The first step of decomposition occurs within the temperature range 30–129 °C and corresponds to the loss of water molecule of hydration with a mass loss of 3.69% (calcd. 3.44%). The second step of decomposition corresponds to the loss of $2H_2O$, HCl and $C_{14}H_{15}N_5O$ fragments with a mass loss 66.16% (calcd. 65.18%). In all complexes the final weight losses are due to the decomposition of the rest of the ligand and metal oxides residue.

3.9. Kinetic studies

The kinetic parameters such as activation energy (E_a), enthalpy (ΔH^*), entropy (ΔS^*), and Gibbs free energy change of the decomposition (ΔG^*) are evaluated graphically by employing the Coats–Redfern [55] and Horowitz–Metzger [56] methods.

3.9.1. Coast-Redfern equation

The Coats–Redfern equation, which is a typical integral method, can represent as:

$$\int_0^a \frac{dx}{(1-\alpha)^n} = \frac{A}{\varphi}\int_{T_1}^{T_2} \exp\left(-\frac{E_a}{RT}\right)dt. \quad (1)$$

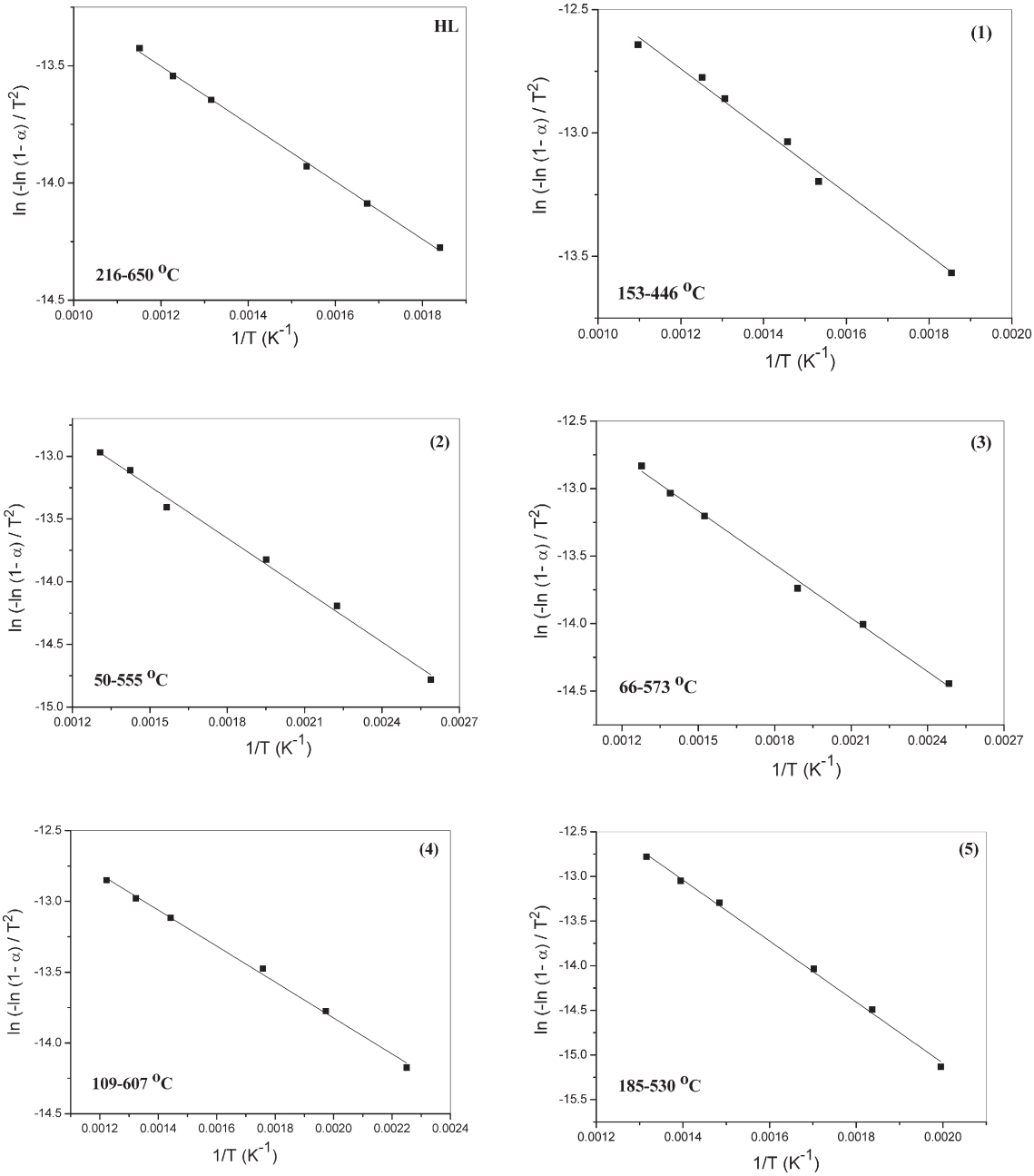

Fig. 12. Coats–Redfern (CR) of ligand (HL) and its metal complexes (1–5).

For convenience of integration, the lower limit T_1 usually taken as zero. This equation on integration gives:

$$\ln\left[-\frac{\ln(1-\alpha)}{T^2}\right] = -\frac{E_a}{RT} + \ln\left[\frac{AR}{\varphi E_a}\right]. \quad (2)$$

A plot of left-hand side (LHS) against $1/T$ was drawn (Fig. 12). E_a is the energy of activation and calculated from the slop and A in (s^{-1}) from the intercept value. The entropy of activation calculated by using the equation:

$$\Delta S^* = 2.303\left[\log\left(\frac{Ah}{k_B T_s}\right)\right]R \quad (3)$$

where k_B is the Boltzmann constant, h is the Plank's constant and T_s is the TG peak temperature.

3.9.2. Horowitz–Metzger equation

The Horowitz–Metzger equation is an illustrative of the approximation methods. These authors derived the relation:

$$\log\left[\frac{1-(1-\alpha)^{1-n}}{1-n}\right] = \frac{E_a\theta}{2.303RT_s^2}, \quad for\ n \neq 1 \quad (4)$$

when $n = 1$, the LHS of Eq. (4) would be $\log[-\log(1-\alpha)]$ (Fig. 13). For a first order kinetic process, the Horowitz–Metzger equation may write in the form:

$$\log\left[\log\left(\frac{W_\alpha}{W\gamma}\right)\right] = \frac{E_a\theta}{2.303RT_s^2} - \log 2.303 \quad (5)$$

where $\theta = T - T_s$, $w_\gamma = w_\alpha - w$, w_α = mass loss at the completion reaction; w = mass loss up to time t. The plot of log [log (w_α/w_γ)] vs. θ was

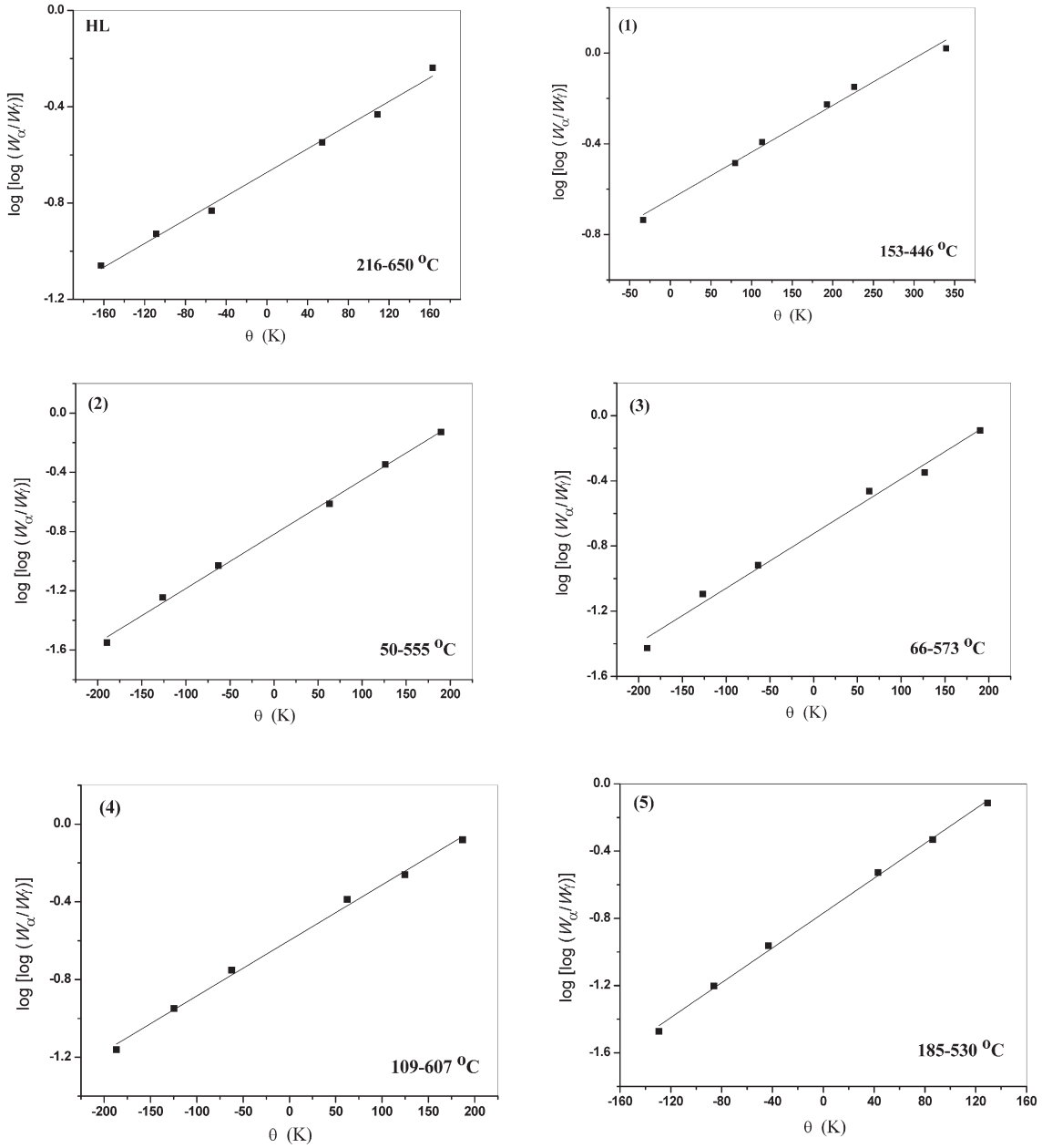

Fig. 13. Horowitz–Metzger (HM) of ligand (HL) and its metal complexes (1–5).

Table 6
Kinetic parameters of HL ligand and its metal complexes*.

Compound	Decomposition temperature (°C)	Method	Parameters					Correlation coefficient (r)
			E_a (kJ mol^{-1})	A (s^{-1})	ΔS^a (J mol^{-1} K^{-1})	ΔH^a (kJ mol^{-1})	ΔG^a (kJ mol^{-1})	
HL	216–650	CR	10.2	1.23E−03	−3.08E+02	4.35	222	0.99818
		HM	24.2	5.94E−02	−2.76E+02	18.3	213	0.99276
1	153–446	CR	10.5	2.79E−03	−2.99E+02	5.71	177	0.99005
		HM	13.0	1.22E−02	−2.87E+02	8.24	173	0.98848
2	50–555	CR	11.5	3.25E−03	−2.98E+02	6.69	178	0.9939
		HM	23.2	1.80E−01	−2.65E+02	18.4	171	0.99675
3	66–573	CR	11.0	3.06E−03	−2.99E+02	6.06	183	0.99624
		HM	22.5	1.24E−01	−2.68E+02	17.6	176	0.98791
4	109–607	CR	10.6	2.66E−03	−3.00E+02	5.31	195	0.99688
		HM	21.8	7.01E−02	−2.73E+02	16.6	189	0.9956
5	185–530	CR	28.4	1.48E−01	−2.67E+02	23.2	192	0.9973
		HM	39.4	3.68E+00	−2.40E+02	34.2	186	0.99749

[a] Numbers given in Table 1.

Table 7
Antibacterial activity data of HL ligand and its metal complexes[a] (**1–5**). The results are recorded as the diameter of inhibition zone (mm) ± SD.

Compound	Gram positive bacteria		Gram negative bacteria	
	Bacillus subtilis (RCMB 010067)	*Streptococcus pneumoniae* (RCMB 010010)	*Pseudomonas aeruginosa* (RCMB 010043)	*Escherichia coli* (RCMB 010052)
HL	16.4 ± 0.63	14.3 ± 2.1	−ve	13.8 ± 1.5
1	27.2 ± 1.2	23.4 ± 0.34	−ve	22.7 ± 5.8
2	21.3 ± 0.58	19.3 ± 2.1	−ve	18.2 ± 0.19
3	22.3 ± 0.58	20.6 ± 1.2	−ve	19.8 ± 0.72
4	20.4 ± 0.58	17.3 ± 1.2	−ve	16.8 ± 0.72
5	24.2 ± 1.5	22.1 ± 0.58	−ve	20.1 ± 2.1
Ampicillin	32.4 ± 0.3	23.8 ± 0.2	−ve	−ve
Gentamicin	−ve	−ve	17.3 ± 0.1	19.9 ± 0.3

[a] Numbers given in Table 1.

drawn and found to be linear from the slope of which E_a was calculated. The pre-exponential factor, A, calculated from equation:

$$\frac{E_a}{RT_s^2} = \frac{A}{\left[\varphi \exp\left(-\frac{E_a}{RT_s}\right)\right]}. \quad (6)$$

The entropy of activation, ΔS^*, is calculated from Eq. (3). The enthalpy activation, ΔH^*, and Gibbs free energy, ΔG^*, calculated from:

$$\Delta H^* = E_a - RT \quad (7)$$

$$\Delta G^* = \Delta H^* - T\Delta S^*. \quad (8)$$

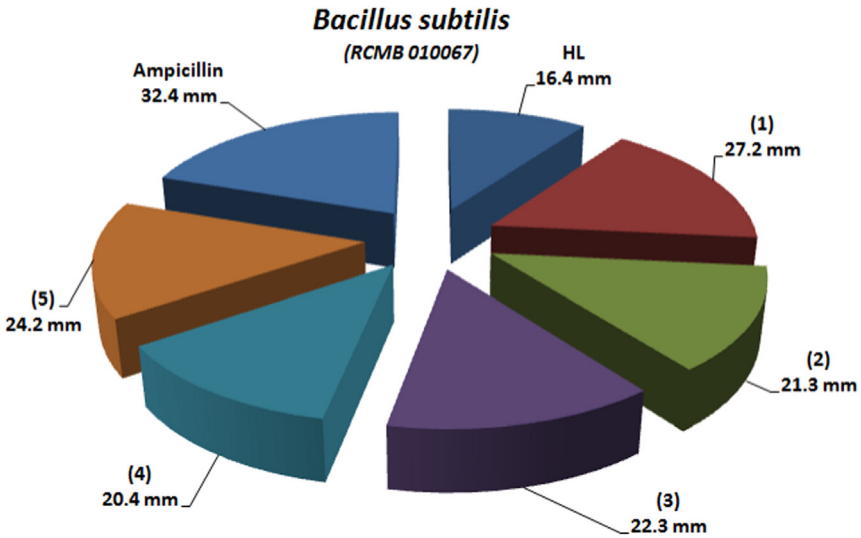

Fig. 14. Antibacterial activity data of HL ligand and its complexes (1–5) against *Bacillus subtilis*.

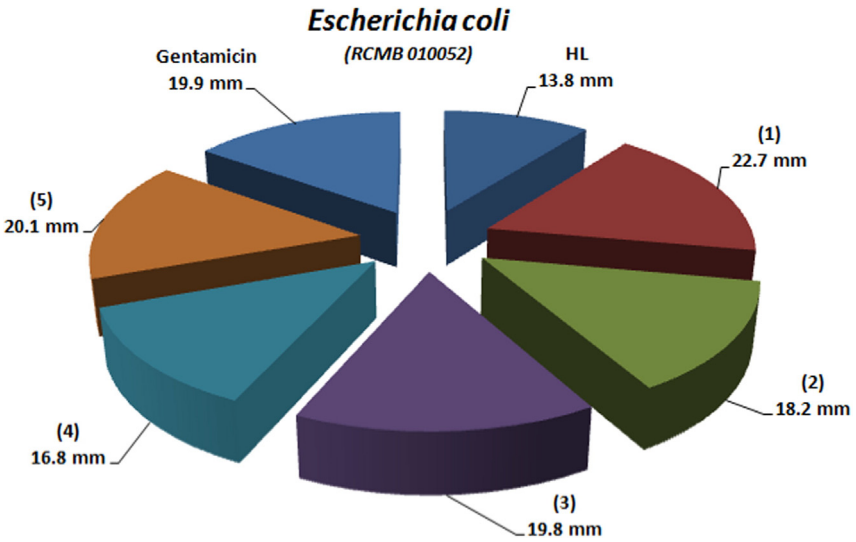

Fig. 15. Antibacterial activity data of HL ligand and its complexes (1–5) against *Escherichia coli*.

The calculated values of E_a, A, ΔS^*, ΔH^* and ΔG^* for the decomposition steps for ligand (HL) and its metal complexes (**1**–**5**) are summarized in Table 6. The kinetic data obtained from the two methods are comparable and can be considered in good agreement with each other.

3.10. Antimicrobial activity

The azodyes of pyrazolone and/or 3-aminophenol are an essential structural requirement for biological activity [8]. Several azodye compounds and their metal complexes have been reported to possess remarkable antibacterial and antifungal activities [1,4,13]. The antimicrobial action of azodye compounds may be significantly enhanced by the presence of azo group which have chelating properties. These properties may be used in metal transport across the bacterial membranes or to attach to the bacterial cells at a specific site from which it can interfere with their growth [8]. Despite the importance of studying the antibacterial and antifungal activities of 4-(2,3-dimethyl-1-phenylpyrazol-5-one azo)-3-aminophenol in biological applications, to the best of our knowledge no studies on the antimicrobial activities have been done.

The antibacterial and antifungal activities of the ligand (HL) and its metal complexes **(1–5)** are tested against four bacteria and two fungi organisms. The used organisms in the present investigation included Gram positive bacteria (*B. subtilis* and *S. pneumoniae*), Gram negative bacteria (*E. coli* and *P. aeruginosa*) and fungi (*A. fumigatus* and *C. albicans*). The results of the antibacterial activity of the ligand (HL) and its metal complexes **(1–5)** are recorded in Table 7. It was found that all the compounds have antibacterial activity against Gram positive bacteria; namely *B. subtilis* (Fig. 14) and *S. pneumonia*, when compared with gentamicin. The ligand (HL) and its metal complexes **(1–5)** were found to have no antibacterial activity against Gram negative bacterium; namely, *P. aeruginosa*, but have antibacterial activity against *E. coli*, when compared with ampicillin as shown in Fig. 15.

The antifungal activity of HL and its complexes **(1–5)** were reported and they were found to have antifungal activity against *A. fumigatus* as shown in Fig. 16 and Table 8. The HL ligand, complexes **(2)** and **(4)** have no antifungal activity against *C. albicans*, while the complexes **(1), (3)** and **(5)** have antifungal activity against *C. albicans* and inhibition zone is 19.6, 15.7 and 17.1 mm, respectively.

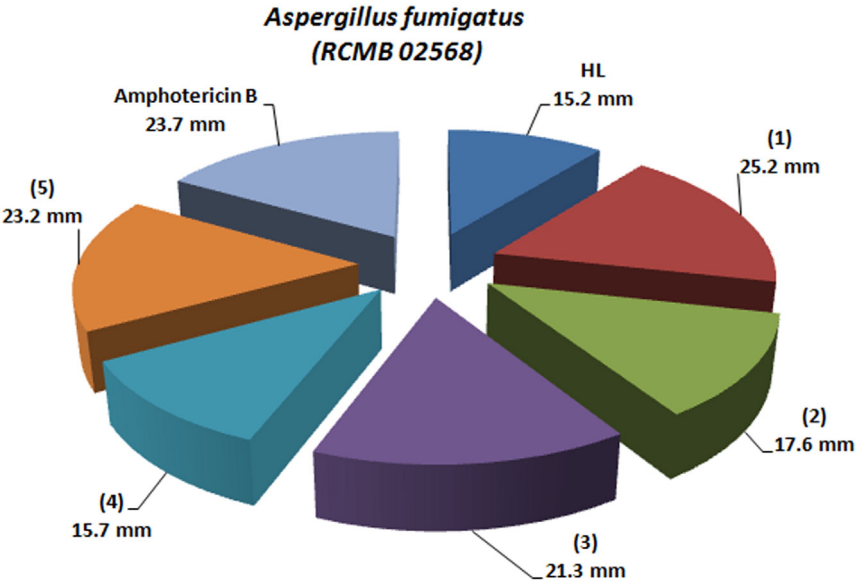

Fig. 16. Antifungal activity data of HL ligand and its complexes (1–5) against *Aspergillus fumigatus*.

Table 8
Antifungal activity data of HL ligand and its metal complexes[a] (**1–5**). The results are recorded as the diameter of inhibition zone (mm) ± SD.

Compound	*Aspergillus fumigatus* (RCMB 02568)	*Candida albicans* (RCMB 05036)
HL	15.2 ± 1.5	−ve
1	25.2 ± 0.72	19.6 ± 0.63
2	17.6 ± 0.63	−ve
3	21.3 ± 1.2	15.7 ± 1.5
4	15.7 ± 2.1	−ve
5	23.2 ± 1.2	17.1 ± 0.63
Amphotericin B	23.7 ± 0.1	25.4 ± 0.1

[a] Numbers given in Table 1.

On comparing the antimicrobial activity of the ligand and its complexes with the standard drugs (ampicillin, gentamicin and amphotericin B), the following results are obtained:

- All complexes have high antimicrobial activities than the ligand (HL).
- Complex **(1)** has the highest antimicrobial activities (except against *P. aeruginosa*) than the other metal complexes.
- Complexes **(1)** and **(5)** have high effect than gentamicin; as standard drug against *E. coli*.
- Complex **(1)** has high effect than amphotericin B; as standard drug against *Aspergillus fumigatus*.
- The antimicrobial activity of the compounds against Gram positive bacteria (*B. subtilis* and *S. pneumoniae*), Gram negative bacteria (*Escherichia coli*) and fungus (*A. fumigatus*) follows the order complex **(1)** > complex **(5)** > complex **(3)** > complex **(2)** > complex **(4)** > HL.

4. Conclusion

The structures of the ligand and its metal complexes were confirmed by the elemental analyses, IR, ^{1}H NMR, mass spectra, molar conductance, magnetic, ESR, UV- vis and thermal analysis. Therefore, from the IR spectra, it was found that the ligand (HL) acts as monobasic tridentate through the (—N═N), enolic (C—O)$^-$ and oxygen keto moiety groups forming a five/six-membered structures. Octahedral geometric structures are suggested for all the complexes. The thermal properties of the ligand and its complexes **(1–5)** were investigated by thermogravimetry analysis (TG) and the calculated values of E_a, A, ΔS^*, ΔH^* and ΔG^* for the decomposition steps for ligand (HL) and its metal complexes (**1–5**) are discussed. The trend $g_{||} > g_{\perp} > g_e$ (2.0023) observed for complex **(4)** shows that the unpaired electron is localized in d_{x2-y2} orbital of the Cu(II) ion and the spectrum features are characteristics of axial symmetry. The divalent metal complexes shows binding energies in the ascending order complex **(5)** < complex **(2)** < complex **(3)** < complex **(4)**. All of the tested compounds showed various remarkable antimicrobial activity against *Bacillus subtilis*, *S. pneumoniae*, *E. coli* and *A. fumigatus*. Only complexes **(1)**, **(3)** and **(5)** showed antifungal effect against *C. albicans*.

Acknowledgement

The authors would like to thank Prof. Dr. M.I. Abou-Dobara, Botany Department, Faculty of Science, Damietta University, Egypt for his help during the research.

Appendix A. Supplementary data

Supplementary data to this article can be found online at http://dx.doi.org/10.1016/j.molliq.2016.02.026.

References

[1] M.A. Diab, A.Z. El-Sonbati, A.A. El-Bindary, G.G. Mohamed, Sh.M. Morgan, Res. Chem. Intermed. 41 (2015) 9029–9066.
[2] N.A. El-Ghamaz, A.Z. El-Sonbati, M.A. Diab, A.A. El-Bindary, G.G. Mohamed, Sh.M. Morgan, Spectrochim. Acta A 147 (2015) 200–211.
[3] A.Z. El-Sonbati, G.G. Mohamed, A.A. El-Bindary, W.M.I. Hassan, M.A. Diab, Sh.M. Morgan, A.K. Elkholy, J. Mol. Liq. 212 (2015) 487–502.
[4] A.Z. El-Sonbati, M.A. Diab, A.A. El-Bindary, G.G. Mohamed, Sh.M. Morgan, Inorg. Chim. Acta 430 (2015) 96–107.
[5] A.Z. El-Sonbati, G.G. Mohamed, A.A. El-Bindary, W.M.I. Hassan, A.K. Elkholy, J. Mol. Liq. 209 (2015) 625–634.
[6] A.A. El-Bindary, A.Z. El-Sonbati, M.A. Diab, Sh.M. Morgan, J. Mol. Liq. 201 (2015) 36–42.
[7] A.A. El-Bindary, M.A. Hussein, R.A. El-Boz, J. Mol. Liq. 211 (2015) 256–267.
[8] A.Z. El-Sonbati, M.A. Diab, A.A. El-Bindary, A.M. Eldesoky, Sh.M. Morgan, Spectrochim. Acta A 135 (2015) 774–791.
[9] Z. Seferoglu, N. Ertan, Russ. J. Org. Chem. 43 (2007) 1035–1041.
[10] M.I. Abou-Dobara, A.Z. El-Sonbati, Sh.M. Morgan, World J. Microbiol. Biotechnol. 29 (2013) 119–126.
[11] M.A. Diab, A.Z. El-Sonbati, A.A. El-Bindary, A.M. Barakat, Spectrochim. Acta A 116 (2013) 428–439.
[12] M.M. Ghoneim, A.Z. El-Sonbati, A.A. El-Bindary, M.A. Diab, L.S. Serag, Spectrochim. Acta A 140 (2015) 111–131.
[13] A.Z. El-Sonbati, M.A. Diab, A.A. El-Bindary, Sh.M. Morgan, Spectrochim. Acta A 127 (2014) 310–328.
[14] A.Z. El-Sonbati, A.F. Shoair, A.A. El-Bindary, A.S. Mohamed, J. Mol, Liq. 209 (2015) 635–647.
[15] A.Z. El-Sonbati, M.A. Diab, A.A. El-Bindary, Sh.M. Morgan, Inorg. Chim. Acta 404 (2013) 175–187.
[16] A.S. Salman, A. Abdel-Aziem, M.J.S. Alkubbat, Intern. J. Org. Chem. 5 (2015) 15–28.
[17] P.W. Selwood, Magnetic chemistry, Interscience Pub. Inc. New York (1956).
[18] M.A. Quraishi, R. Sardar, D. Jamal, Mater. Chem. Phys. 71 (2001) 309–313.
[19] N.A. El-Ghamaz, A.Z. El-Sonbati, M.A. Diab, A.A. El-Bindary, M.K. Awad, Sh.M. Morgan, Mater. Sci. Semicond. Process. 19 (2014) 150–162.
[20] A.D. Becke, J. Chem. Phys. 98 (1993) 5648–5652.
[21] B.G. Johnson, M.J. Frisch, Chem. Phys. Lett. 216 (1993) 133–140.
[22] C. Lee, W. Yang, R.G. Parr, Phys. Rev. B 37 (1988) 785–789.
[23] A.D. McLean, G.S. Chandler, Contracted Gaussian-basis sets for molecular calculations. 1. 2nd row atoms, Z = 11–18, J. Chem. Phys. 72 (1980) 5639–5648.
[24] T.H. Dunning Jr. and P.J. Hay, in Modern Theoretical Chemistry, Ed. H. F. Schaefer III, 3 (Plenum, New York, 1977) 1–28.
[25] P.J. Hay, W.R. Wadt, Ab initio effective core potentials for molecular calculations — potentials for K to Au including the outermost core orbitals, J. Chem. Phys. 82 (1985) 299–310.
[26] M.J. Frisch, G.W. Trucks, H.B. Schlegel, G.E. Scuseria, M.A. Robb, J.R. Cheeseman, G. Scalmani, V. Barone, B. Mennucci, G.A. Petersson, H. Nakatsuji, M. Caricato, X. Li, H.P. Hratchian, A.F. Izmaylov, J. Bloino, G. Zheng, J.L. Sonnenberg, M. Hada, M. Ehara, K. Toyota, R. Fukuda, J. Hasegawa, M. Ishida, T. Nakajima, Y. Honda, O. Kitao, H. Nakai, T. Vreven, J.A. Montgomery, Jr., J.E. Peralta, F. Ogliaro, M. Bearpark, J.J. Heyd, E. Brothers, K.N. Kudin, V.N. Staroverov, T. Keith, R. Kobayashi, J. Normand, K. Raghavachari, A. Rendell, J. C. Burant, S. S. Iyengar, J. Tomasi, M. Cossi, N. Rega, J. M. Millam, M. Klene, J. E. Knox, J. B. Cross, V. Bakken, C. Adamo, J. Jaramillo, R. Gomperts, R. E. Stratmann, O. Yazyev, A.J. Austin, R. Cammi, C. Pomelli, J.W. Ochterski, R.L. Martin, K. Morokuma, V.G. Zakrzewski, G.A. Voth, P. Salvador, J.J. Dannenberg, S. Dapprich, A.D. Daniels, O. Farkas, J.B. Foresman, J.V. Ortiz, J. Cioslowski, D.J. Fox, Gaussian, Inc., Wallingford CT, 2010.
[27] T. Keith, J. Millam (Eds.), GaussView, Version 5, R. Dennington, Semichem Inc., Shawnee Mission KS, 2009.
[28] L. Antonov, S. Kawauchi, M. Satoh, J. Kamiyama, Dyes Pigments 38 (1998) 157–164.
[29] M. Cheriyan, K. Mohanan, Asian J. Chem. 19 (2007) 2831–2838.
[30] A.S. Abd-El-Aziz, T.H. Afifi, Fyes Pigm. 70 (2006) 8–17.
[31] N.A. El-Ghamaz, A.A. El-Bindary, M.A. Diab, A.Z. El-Sonbati, S.G. Nozha, Res. Chem. Intermed. (2015), http://dx.doi.org/10.1007/s11164-015-2164-5.
[32] V. Stefov, V.M. Petrusevski, B. Soptrajanov, J. Mol. Struct. 293 (1993) 97–100.
[33] J. Liang, W. Lipscomb, Biochemistry 28 (1989) 9724–9733.
[34] G.G. Mohamed, Nadia E.A., F.A. El-Gamel, Nour El-Dien, Synth. React. Inorg. Met.-Org. Chem. 31 (2001) 347–358.
[35] M.A. Ali, S.M.M.H. Majumder, R.J. Butcher, J.P. Jasinski, J.M. Jasinski, Polyhedron 16 (1997) 2749–2754.
[36] R. Prasad, P.P. Thankachan, M.T. Thomas, R. Pathak, J. Ind. Chem. Soc. 78 (2001) 28–31.
[37] J. Kohout, M. Hvastijova, J. Kozisek, J.G. Diaz, M. Valko, L. Jager, I. Svoboda, Inorg. Chim. Acta 287 (1999) 186–192.
[38] A. Bury, A.E. Underhill, D.R. Kemp, N.J. O'shea, J.P. Smith, P.S. Gomm, F. Hallway, Inorg. Chim. Acta 138 (1987) 85–89.
[39] J. Manonmani, R. Thirumurugan, M. Kandaswamy, M. Kuppayee, S.S.S. Raj, M.N. Ponnuswamy, G. Shanmugam, H.K. Fun, Polyhedron 19 (2000) 2011–2018.
[40] J. Sanmartin, M.R. Bermejo, A.M.G. Deibe, M. Maneiro, C. Lage, A.J.C. Filho, Polyhedron 19 (2000) 185–192.
[41] V.P. Krzyminiewska, H. Litkowska, W.R. Paryzek, Monatshefte, Fur. Chemie 130 (1999) 243–247.
[42] K. Bertoncello, G.D. Fallon, K.S. Murray, E.R.T. Tiekink, Inorg. Chem. 30 (1991) 3562.
[43] W.J. Sawodny, M. Riederer, Angew. Chem., Int. Ed. 16 (1977) 859–860.
[44] D.R. Zhu, Y. Song, Y. Xu, Y. Zhang, S.S.S. Raj, H.K. Fun, X.Z. You, Polyhedron 19 (2000) 2019–2025.

[45] N.R.S. Kumar, M. Nethiji, K.C. Patil, Polyhedron 10 (1991) 365–371.
[46] D. Kivelson, R. Neiman, J. Chem. Phys. 35 (1961) 149–155.
[47] B. Singh, B.P. Yadav, R.C. Aggarwal, Ind. J. Chem. 23A (1984) 441–446.
[48] S. Balasubramanian, C.N. Krishnan, Polyhedron 5 (1986) 669–675.
[49] B.J. Hathaway, D.E. Billing, Coord. Chem. Rev. 6 (1970) 143–207.
[50] B.J. Hathaway, in: J.N. Bradly, R.D. Gillard (Eds.), Essays in Chemistry, Academic Press, New York 1971, pp. 61–92.
[51] A.Z. El-Sonbati, A.A. El-Bindary, New Polym. Mater. 5 (1996) 51–60.
[52] A.T. Mubarak, A.Z. El-Sonbati, A.A. El-Bindary, Appl. Organomet. Chem. 18 (2004) 212–220.
[53] G.F. Pryce, J. Phys. Chem. 79 (1966) 3549–3557.
[54] M.C.R. Symons, Adv. Phys. Org. Chem. 1 (1963) 283–363.
[55] A.W. Coats, J.P. Redfern, Nature 20 (1964) 68–79.
[56] H.W. Horowitz, G. Metzger, Anal. Chem. 35 (1963) 1464–1468.